ENCI (1)

AD-A285 689

REPORT DOCUMENTATION PAGE

1. REPORT NUMBER Technical Note BN-1178	2. GOVT

4. TITLE (and Subtitle) The Method of Auxiliary Mapping for the Finite Element Solutions of Elasticity Problems Containing Singularities	5. TYPE OF REPORT & PERIOD COVERED Final Life of Contract
	6. PERFORMING ORG. REPORT NUMBER

7. AUTHOR(s) Hae-Soo Oh[1] - Ivo Babuska[2]	8. CONTRACT OR GRANT NUMBER(s) [2] N00014-90-J-1030 (ONR) & DMS-91-20877 (NSF) [1] ASC-9113895 (NSF)

9. PERFORMING ORGANIZATION NAME AND ADDRESS [2]Institute for Physical Science and Technology University of Maryland College Park, MD 20742-2431	10. PROGRAM ELEMENT, PROJECT, TASK AREA & WORK UNIT NUMBERS

11. CONTROLLING OFFICE NAME AND ADDRESS Department of the Navy Office of Naval Research Arlington, VA 22217	12. REPORT DATE September 1994
	13. NUMBER OF PAGES 42

14. MONITORING AGENCY NAME & ADDRESS(if different from Controlling Office)	15. SECURITY CLASS. (of this report)
	15a. DECLASSIFICATION/ DOWNGRADING SCHEDULE

16. DISTRIBUTION STATEMENT (of this Report)

Approved for public release: distribution unlimited

17. DISTRIBUTION STATEMENT (of the abstract entered in Block 20, if different from Report)

DTIC
ELECTE
OCT. 24 1994
B

18. SUPPLEMENTARY NOTES

19. KEY WORDS (Continue on reverse side if necessary and identify by block number)

20. ABSTRACT (

Babuška and Oh have introduced a new approach called the Method of Auxiliary Mapping(MAM), to deal with elliptic boundary value problems with singularities. In this paper this method is extended so that it can handle the plane elasticity problems containing singularities. In order to show the effectiveness, this method is compared with the conventional approach in the framework of the p-version of the finite element method. Moreover, it is demonstrated that this method yields a reasonable solution for those elasticity problems containing strong singularities which even can not be solved by using the h-p version of the finite element method.

MARYLAND

COLLEGE PARK CAMPUS

THE METHOD OF AUXILIARY MAPPING
FOR THE FINITE ELEMENT SOLUTIONS
OF ELASTICITY PROBLEMS CONTAINING SINGULARITIES

by

Hae-Soo Oh

and

Ivo M. Babuška

Technical Note BN-1178

September 1994

INSTITUTE FOR PHYSICAL SCIENCE AND TECHNOLOGY

94-32918

THE METHOD OF AUXILIARY MAPPING FOR THE FINITE ELEMENT SOLUTIONS OF ELASTICITY PROBLEMS CONTAINING SINGULARITIES

Hae-Soo Oh[*]
Department of Mathematics
University of North Carolina at Charlotte
Charlotte, North Carolina 28223

Ivo Babuška[†]
Institute for Physical Science and Technology
University of Maryland
College Park, Maryland 20742

Abstract

Babuška and Oh have introduced a new approach called the Method of Auxiliary Mapping(MAM), to deal with elliptic boundary value problems with singularities. In this paper this method is extended so that it can handle the plane elasticity problems containing singularities. In order to show the effectiveness, this method is compared with the conventional approach in the framework of the p-version of the finite element method. Moreover, it is demonstrated that this method yields a reasonable solution for those elasticiy problems containing strong singularities which even can not be solved by using the h-p version of the finite element method.

1

1 Introduction

In ([8]) and ([30]), we introduce a new approach called the Method of Auxiliary Mapping, to deal with domain singularity and interface singularity, which arise in such elliptic boundary value problems as steady state heat transfer. In this paper, this approach is extended for plane elasticity problems containing singularities.

There are three versions of the finite element method: the h-version, the p-version, and the h-p version. The h-version ([13],[35]) is the standard one, where the degree p of the elements is fixed, usually at a low level, typically with $p = 1, 2$, or 3 and the accuracy is achieved by properly refining the mesh. The p-version ([10], [12], [36]), in contrast, fixes the mesh and achieves better accuracy by increasing the degree p of the elements uniformly or selectively. The h-p version ([4]-[5], [11], [16]-[21]) is a combination of both. In this paper, we are concerned with the p-version of the finite element method.

In the theory and practice of the finite element method, much work has been done to design special approaches to deal with elasticity problems containing singularities ([25],[32],[33],[38]). Singularities occur when the solution domain has corners, abrupt changes in boundary data, or consists of two or more materials. These singularities are called a corner singularity ([9],[15],[27],[34]), a boundary data singularity([29],[37]), and an interface singularity([23],[26],[29],[31]), respectively.

In an effort to provide accurate and economical solutions, many different approaches to deal with singularity in elasticity problems have been attempted over the years. Basically there are three ways the problem is approached: mesh refinement([7],[11],[16],[17], [18], [19], [20],[35]); use of special singular elements([1],[2],[22]); and use of (nonlocal) special singular functions([24]). Expanding the trial space by adding special singular (local or global) functions which mimic the singularities can lead to a more accurate solution, but more problems will be generated, especially in computer coding. Moreover, one must know the structure of the eigenvalues corresponding to the singular points in order to choose proper singular functions. The most popular approach is the mesh refinement, but its success depends on a proper choice of mesh and it also requires longer computing time. Moreover, when the singularity is very strong, as in Example 5.II, this approach cannot give any acceptable results.

In this paper, the Method of Auxiliary Mapping introduced in ([8]) and ([30]) will be modified so that it can efficiently handle the singularities which arise in plane elasticity problems. It will be shown that this new approach yields far better results for elasticity problems containing singularities than do conventional approaches at virtually no extra cost. Moreover, this method gives a reasonable solution for those elasticity problems which even can not be solved by using the h-p version of the Finite Element Method.

This paper is organized as follows: The notations and the model problems to work with are described in §2. In §3, the structure of the corner singularity and basic lemmas are introduced. In §4, the Method of Auxiliary Mapping is explained in the context of plane elasticity, and the improvement of error bounds by Method of Auxiliary Mapping

2

is presented. Various numerical results to demonstrate effectiveness of our method are given in §5. These include an especially remarkable success in Examples 5.I and 5.II and MAM's handling of interface singularities caused by an abrupt change in material properties. Finally, the concluding remarks are given in §6.

2 Preliminary

2.1 The Notation

For $\Omega \in \mathcal{R}^2$ a polygonal domain with boundary $\partial\Omega$, we let $L_2(\Omega) = H^0(\Omega), H^k(\Omega), H_0^k(\Omega)$, $k \geq 0$ integer, denote the usual Sobolev spaces. For $u \in H^k(\Omega)$ we denote by $\|u\|_{k,\Omega}$ and $|u|_{k,\Omega}$, the usual norm and seminorm, respectively.

In elasticity, the state variable is the displacement vector denoted by $\{u\} = \{u_x(x,y), u_y(x,y)\}^T$ and the flux is the stress tensor denoted by $\{\sigma^{(u)}\} = \{\sigma_x^{(u)}, \sigma_y^{(u)}, \tau_{xy}^{(u)}\}^T$. Let $\{\epsilon^{(u)}\} = \{\epsilon_x^{(u)}, \epsilon_y^{(u)}, \gamma_{xy}^{(u)}\}^T$ be the strain tensor. Then the strain-displacement and the stress-strain relations are given by

$$\{\epsilon^{(u)}\} = [D]\{u\} \text{ and } \{\sigma^{(u)}\} = [E]\{\epsilon^{(u)}\} \tag{1}$$

respectively, where $[D]$ is the differential operator matrix:

$$[D] = \begin{bmatrix} \dfrac{\partial}{\partial x} & 0 \\ 0 & \dfrac{\partial}{\partial y} \\ \dfrac{\partial}{\partial y} & \dfrac{\partial}{\partial x} \end{bmatrix}$$

and $[E] = [E_{ij}], 1 \leq i, j \leq 3$, is the symmetric positive definite matrix of material constants. For an isotropic elastic body, in the case of plane stress,

$$[E] = \frac{E}{1-\nu^2} \begin{bmatrix} 1 & \nu & 0 \\ \nu & 1 & 0 \\ 0 & 0 & \dfrac{1-\nu}{2} \end{bmatrix},$$

where E is the module of elasticity and $\nu(0 \leq \nu < 1/2)$ is Poisson's ratio.

The equilibrium equations of elasticity are

$$[D]^T\{\sigma^{(u)}\}(x,y) + \{f\}(x,y) = 0, \quad (x,y) \in \Omega, \tag{2}$$

where $\{f\} = \{f_x(x,y), f_y(x,y)\}^T$ is the vector of internal sources representing the body force per unit area.

3

2.2 The Model Problem

Introducing the relations (1) into (2), the equilibrium equations can be expressed in terms of the displacement vector $\{u\}$. Consider the following system of the partial differential equations in terms of the displacement vector:

$$[D]^T[E][D]\{u\}(x,y) + \{f\}(x,y) = 0, \quad (x,y) \in \Omega \tag{3}$$

subject to the following boundary conditions:

$$[N]\{\sigma^{(u)}\}(s) = \{\tilde{T}\}(s) = \{\tilde{T}_x(s), \tilde{T}_y(s)\}^T, \quad s \in \Gamma^1, \tag{4}$$

$$\{u\}(s) = \{\tilde{u}\}(s) = \{\tilde{u}_x(s), \tilde{u}_y(s)\}^T, \quad s \in \Gamma^2, \tag{5}$$

where $\Gamma^1 \cup \Gamma^2 = \partial\Omega$, $\{n_x, n_y\}^T$ is a unit vector normal to the boundary $\partial\Omega$ of the domain Ω and

$$[N] = \begin{bmatrix} n_x & 0 & n_y \\ 0 & n_y & n_x \end{bmatrix}.$$

Let $H_D^1(\Omega) = \{\{w\} = \{w_x, w_y\} \in [H^1(\Omega)]^2 : \{w\} = 0 \text{ on } \Gamma^2\}$. Then, as usual, the variational form of (3)-(5) is as follows: find the vector $\{u\}$ such that $u_x, u_y \in H^1(\Omega), \{u\} = \{\tilde{u}\}$ on Γ^2 and

$$\mathcal{B}(\{u\}, \{v\}) = \mathcal{F}(\{v\}), \text{ for all } \{v\} \in H_D^1(\Omega), \tag{6}$$

where

$$\mathcal{B}(\{u\}, \{v\}) = \int_\Omega ([D]\{v\})^T [E] ([D]\{u\}) dx dy, \tag{7}$$

$$\mathcal{F}(\{v\}) = \int_\Omega \{v\}^T \{f\} dx dy + \oint_{\Gamma^1} \{v\}^T \{\tilde{T}\} ds. \tag{8}$$

By the strain energy of the displacement vector $\{u\}$ we mean $\mathcal{U}(\{u\}) = (1/2)\mathcal{B}(\{u\}, \{u\})$.

The finite element approximation of the solution of (6) is to construct approximations of each component of the vector $\{u\}$. We denote the basis functions defined on Ω by $\Psi_i(x,y), i = 1, 2, ..., n$. The components of the displacement vector in term of basis functions Ψ_i are of the form:

$$u_x(x,y) = \sum_{i=1}^n a_i \Psi_i(x,y)$$

$$u_y(x,y) = \sum_{i=1}^n a_{n+i} \Psi_i(x,y).$$

where $a_i (i = 1, 2, ..., 2n)$ are called the amplitudes of the basis functions Ψ_i. Let

$$\{\Psi_i\} = \left\{ \begin{array}{c} \Psi_i(x,y) \\ 0 \end{array} \right\}, i = 1, 2, ..., n \tag{9}$$

$$\{\Psi_i\} = \left\{ \begin{array}{c} 0 \\ \Psi_{i-n}(x,y) \end{array} \right\}, i = n+1, n+2, ..., 2n. \tag{10}$$

4

Then $\{u\}$ can be written as:

$$\{u\} = \sum_{i=1}^{2n} a_i \{\Psi_i\}.$$

Moreover we have the following:

Lemma 2.1 *The bilinear form $\mathcal{B}(\{u\}, \{v\})$ on an element e becomes*

$$\int_e (\nabla \Psi_j)^T \begin{bmatrix} E_{11} & E_{13} \\ E_{31} & E_{33} \end{bmatrix} (\nabla \Psi_i) \; \text{if} \; \{v\} = \{\Psi_i, 0\}^T \; \text{and} \; \{u\} = \{\Psi_j, 0\}^T,$$

$$\int_e (\nabla \Psi_j)^T \begin{bmatrix} E_{33} & E_{32} \\ E_{23} & E_{22} \end{bmatrix} (\nabla \Psi_i) \; \text{if} \; \{v\} = \{0, \Psi_i\}^T \; \text{and} \; \{u\} = \{0, \Psi_j\}^T,$$

$$\int_e (\nabla \Psi_j)^T \begin{bmatrix} E_{13} & E_{12} \\ E_{33} & E_{32} \end{bmatrix} (\nabla \Psi_i) \; \text{if} \; \{v\} = \{\Psi_i, 0\}^T \; \text{and} \; \{u\} = \{0, \Psi_j\}^T,$$

$$\int_e (\nabla \Psi_j)^T \begin{bmatrix} E_{31} & E_{33} \\ E_{21} & E_{23} \end{bmatrix} (\nabla \Psi_i) \; \text{if} \; \{v\} = \{0, \Psi_i\}^T \; \text{and} \; \{u\} = \{\Psi_j, 0\}^T.$$

3 The Corner Singularities

The accuracy of the finite element approximation depends on the regularity of the true solution ([6]). In the presence of singularity the solution of (3)-(5) has a low regularity. In this section the structure of the singularity due to nonsmoothness of the domain will be investigated. For this purpose the equations of elasticity (3) will be localised by restricting (3) on a neighborhood of a singularity of the domain Ω.

3.1 The behavior of a solution in the vicinity of nonsmooth boundary

Let us consider the equations of elasticity (3) in the vicinity of a corner shown in Fig. 3.1. When the body force is neglected, the equations of elasticity in the polar coordinates system can be written as

$$(\zeta + 2\mu)\frac{\partial}{\partial r}\{\frac{\partial u_r}{\partial r} + \frac{1}{r}\frac{\partial u_\theta}{\partial \theta} + \frac{u_r}{r}\} - \mu\frac{1}{r}\frac{\partial}{\partial \theta}\{\frac{\partial u_\theta}{\partial r} - \frac{1}{r}\frac{\partial u_r}{\partial \theta} + \frac{u_\theta}{r}\} = 0 \qquad (11)$$

$$(\zeta + 2\mu)\frac{1}{r}\frac{\partial}{\partial \theta}\{\frac{\partial u_r}{\partial r} + \frac{1}{r}\frac{\partial u_\theta}{\partial \theta} + \frac{u_r}{r}\} + \mu\frac{\partial}{\partial r}\{\frac{\partial u_\theta}{\partial r} - \frac{1}{r}\frac{\partial u_r}{\partial \theta} + \frac{u_\theta}{r}\} = 0 \qquad (12)$$

where

$$\mu = \frac{E}{2(1+\nu)} \; \text{and} \; \zeta = \frac{\nu E}{(1+\nu)(1-2\nu)}, \qquad (13)$$

which characterize materials. Here E is the module of elasticity and ν is Poisson's ratio.

The radial and tangential stresses on the wedge surfaces are

$$\sigma_{\theta\theta} = \zeta\left(\frac{\partial u_r}{\partial r} + \frac{1}{r}\frac{\partial u_\theta}{\partial \theta} + \frac{u_r}{r}\right) + 2\mu\left(\frac{1}{r}\frac{\partial u_\theta}{\partial \theta} + \frac{u_r}{r}\right), \tag{14}$$

$$\sigma_{r\theta} = \mu\left(\frac{\partial u_\theta}{\partial r} + \frac{1}{r}\frac{\partial u_r}{\partial \theta} - \frac{u_\theta}{r}\right). \tag{15}$$

Let us consider the solutions of (11) and (12) in the following form:

$$u_r = r^\lambda f(\theta), \tag{16}$$

$$u_\theta = r^\lambda g(\theta). \tag{17}$$

Substitution of these forms into (11) and (12) gives a system of ordinary differential equations in f and g. One can see that the solution of this system has the form

$$\begin{aligned} f = {} & A_1 \cos\left[(1+\lambda)\theta\right] + A_2 \sin\left[(1+\lambda)\theta\right] \\ & + A_3 \cos\left[(1-\lambda)\theta\right] + A_4 \sin\left[(1-\lambda)\theta\right], \end{aligned} \tag{18}$$

$$\begin{aligned} g = {} & A_2 \cos\left[(1+\lambda)\theta\right] - A_1 \sin\left[(1+\lambda)\theta\right] \\ & + \eta A_4 \cos\left[(1-\lambda)\theta\right] - \eta A_3 \sin\left[(1-\lambda)\theta\right], \end{aligned} \tag{19}$$

where $\eta = (3 + \lambda - 4\nu)/(3 - \lambda - 4\nu)$. Then displacements and stresses in the vicinity of the corner will be expressed as

$$\begin{aligned} r^{-\lambda}u_r = {} & A_1 \cos\left[(1+\lambda)\theta\right] + A_2 \sin\left[(1+\lambda)\theta\right] \\ & + A_3 \cos\left[(1-\lambda)\theta\right] + A_4 \sin\left[(1-\lambda)\theta\right], \end{aligned} \tag{20}$$

$$\begin{aligned} r^{-\lambda}u_\theta = {} & A_2 \cos\left[(1+\lambda)\theta\right] - A_1 \sin\left[(1+\lambda)\theta\right] \\ & + \eta A_4 \cos\left[(1-\lambda)\theta\right] - \eta A_3 \sin\left[(1-\lambda)\theta\right], \end{aligned} \tag{21}$$

$$\begin{aligned} \mu^{-1}r^{1-\lambda}\sigma_{\theta\theta} = {} & -2\lambda A_1 \cos\left[(1+\lambda)\theta\right] - 2\lambda A_2 \sin\left[(1+\lambda)\theta\right] \\ & -(1+\lambda)(1-\eta)A_3 \cos\left[(1-\lambda)\theta\right] \\ & -(1+\lambda)(1-\eta)A_4 \sin\left[(1-\lambda)\theta\right], \end{aligned} \tag{22}$$

$$\begin{aligned} \mu^{-1}r^{1-\lambda}\sigma_{r\theta} = {} & -2\lambda A_1 \sin\left[(1+\lambda)\theta\right] + 2\lambda A_2 \cos\left[(1+\lambda)\theta\right] \\ & -(1-\lambda)(1-\eta)A_3 \sin\left[(1-\lambda)\theta\right] \\ & -(1-\lambda)(1-\eta)A_4 \cos\left[(1-\lambda)\theta\right]. \end{aligned} \tag{23}$$

From now on, "the wedge angle α" stands for "the wedge angle 2α". Let us label the boundary conditions along the boundaries $\theta = \alpha$ and $\theta = -\alpha$ of a wedge-shaped region bounded by radii $\theta = \pm\alpha$, as shown in Fig. 3.1, as follows:

$$BC_1 : \quad u_\theta = u_r = 0,$$
$$BC_2 : \quad \sigma_{\theta\theta} = \tau_{r\theta} = 0,$$
$$BC_3 : \quad u_\theta = \tau_{r\theta} = 0.$$

6

In order to determine the eigenvalues λ and the constants A_1, A_2, A_3, A_4, for various boundary conditions on the boundary surfaces $\theta = \pm\alpha$, these boundary conditions are applied to the equations (20)-(23). Then because of the given boundary conditions, we obtain the following trigonometric equations to determine the eigenvalues λ (see, [25] and [32] for details):

$$
\begin{aligned}
\sin(2\lambda\alpha) &= \pm\lambda\sin(2\alpha)/C & &\text{if } BC_1\text{-}BC_1 \text{ is imposed,} \\
\sin(2\lambda\alpha) &= \pm\lambda\sin(2\alpha) & &\text{if } BC_2\text{-}BC_2 \text{ is imposed,} \\
\sin(2\lambda\alpha) &= \pm\sin(2\alpha) & &\text{if } BC_3\text{-}BC_3 \text{ is imposed,} \\
\sin^2(2\lambda\alpha) &= (1+\lambda)^2/4\lambda - \lambda^2\sin^2(2\alpha)/C & &\text{if } BC_1\text{-}BC_2 \text{ is imposed,} \\
\sin(4\lambda\alpha) &= -\lambda\sin(4\alpha) & &\text{if } BC_2\text{-}BC_3 \text{ is imposed,} \\
\sin(4\lambda\alpha) &= \lambda\sin(4\alpha)/C & &\text{if } BC_1\text{-}BC_3 \text{ is imposed,}
\end{aligned}
$$

where $C = 3 - 4/\nu$ for plane strain and $C = (3 - \nu)/(1 + \nu)$ for the plane stress and $BC_i\text{-}BC_j$ means that BC_i is on one side and BC_j is on the other side of the boundary surfaces, $\theta = \pm\alpha$.

These trigonometric equations could have complex roots as well as real roots. For various wedge angles α and for various boundary conditions, $\min\{Re(\lambda)\}$ are computed in (§3.8 of [32]). In particular, if the condition BC_3 is imposed on both of $\theta = \pm\alpha$, $0 < \alpha < 90°$, then the smallest real eigenvalue λ ($\min\{Re(\lambda)\}$) can be arbitrary small as α goes to $90°$. Fig. 3.2 shows the smallest real root λ of the trigonometric equation: $\sin 2\lambda\alpha = \sin 2\alpha$, for $75° \leq \alpha \leq 90°$. In such cases, the singularities are too strong to obtain any reasonable approximations by standard numerical approaches. These cases will be elaborated in Example 5.II.
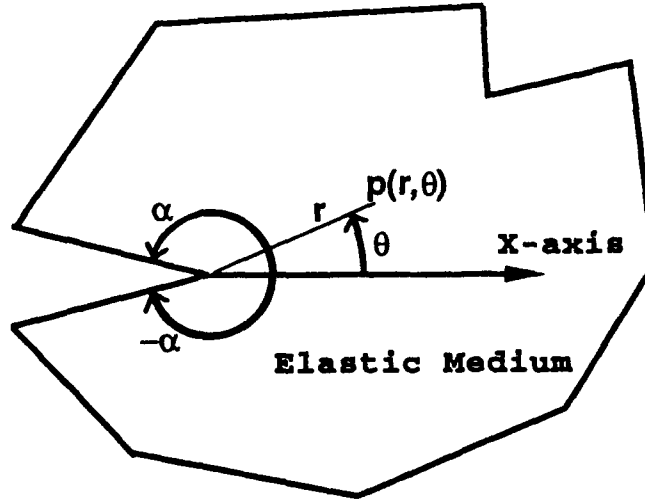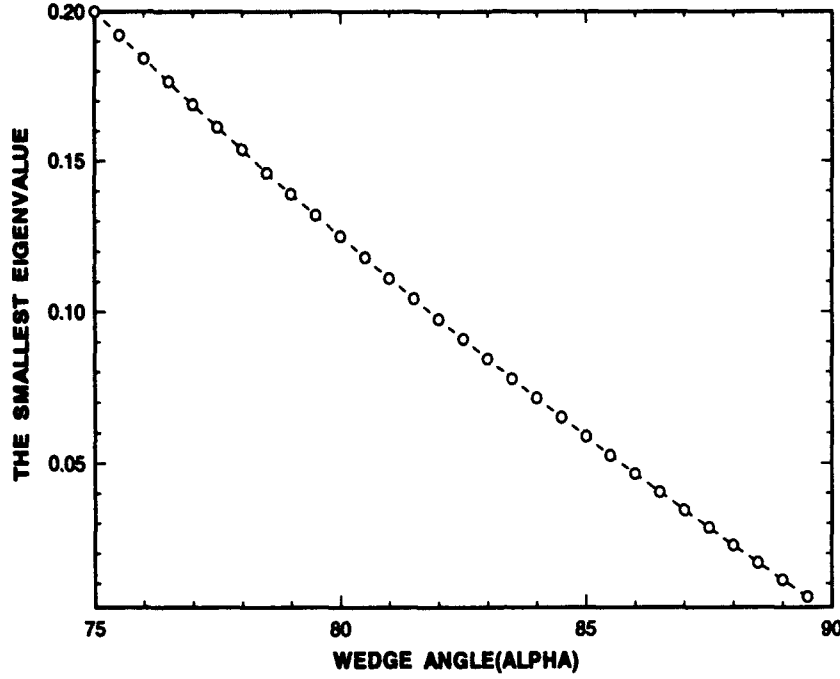

Fig. 3.1. The vicinity of a singularity with wedge angle α.

Fig. 3.2. The smallest eigenvalue versus the wedge angle α when the normal displacement and tangential traction are zero along the boundary surfaces, $\theta = \pm\alpha$.

3.2 The Computation of the Bilinear form on the Regions transformed by Auxiliary Mappings

Now we consider an auxiliary mapping which will be used to describe our new approach to deal with elasticity problems containing singularities. Let $z = x + iy$ and $\zeta = \xi + i\eta$. Let

$$S = \{(r,\theta): \quad 0 \leq r \leq R, a \leq \theta \leq b\}, \tag{24}$$

$$S^* = \{(r^*,\theta^*): \quad 0 \leq r^* \leq R^{1/\beta}, a/\beta \leq \theta^* \leq b/\beta\} \tag{25}$$

be two circular sectors in the z-plane and the ζ-plane respectively. Suppose $\varphi^\beta : S^* \to S$ is the conformal mapping defined by

$$z = \varphi^\beta(\zeta) = \zeta^\beta \tag{26}$$

and let ψ be the inverse function of φ^β, then the determinants of their Jacobians are

$$|J(\varphi^\beta)| = \beta^2 (r^*)^{2(\beta-1)} \text{ and } |J(\psi)| = \frac{1}{\beta^2} r^{2(1-\beta)/\beta} \tag{27}$$

8

respectively. We denote the shifted function onto S^* of a function $f : S \longrightarrow R$ by the conformal mapping φ^β by $\hat{f} = f \circ \varphi^\beta$.

The following lemma was proved in [30] and it will play a key role in the Method of Auxiliary Mapping.

Lemma 3.1. *For $u, v \in H^1(S)$, we have*

$$\int_S (\nabla u)^T \begin{bmatrix} a_{11} & a_{12} \\ a_{21} & a_{22} \end{bmatrix} \nabla v \, dx \, dy = \int_{S^*} (\nabla \hat{u})^T \begin{bmatrix} q_{11} & q_{12} \\ q_{21} & q_{22} \end{bmatrix} \nabla \hat{v} \, d\xi \, d\eta \qquad (28)$$

where

$$\begin{cases} t = & (1 - \beta)\theta^* \\ q_{11} = & a_{11} \cos^2 t + a_{22} \sin^2 t - (a_{21} + a_{12}) \sin t \cos t \\ q_{12} = & (a_{11} - a_{22}) \sin t \cos t - a_{21} \sin^2 t + a_{12} \cos^2 t \\ q_{21} = & (a_{11} - a_{22}) \sin t \cos t - a_{12} \sin^2 t + a_{21} \cos^2 t \\ q_{22} = & a_{11} \sin^2 t + a_{22} \cos^2 t + (a_{12} + a_{21}) \sin t \cos t, \end{cases}$$

and (r^*, θ^*) represents the polar coordinates of points in S^*. For $v \in H^1(S)$ and $f \in H^0(S)$, we have

$$\int_S f(x, y) v(x, y) \, dx \, dy = \int_{S^*} \beta^2 (\xi^2 + \eta^2)^{\beta-1} \hat{f}(\xi, \eta) \hat{v}(\xi, \eta) \, d\xi \, d\eta. \qquad (29)$$

Remark 3.2. (1) From Lemma 2.1, the bilinear form $\mathcal{B}(\{\Psi_i\}, \{\Psi_j\})$ for the basis vector functions has the same form as the left hand side of the integrals in Lemma 3.1. Thus, the local stiffness matrices on S by the basis vector functions (9)-(10) are the same as the local stiffness matrices on S^* by the mapped basis vector, $\{\widehat{\Psi_i}\} = \{\Psi_i\} \circ \varphi^\beta$.

(2) Constraining the stiffness matrices on the elements in S due to the non-homogeneous essential boundary conditions $\{\tilde{u}_x, \tilde{u}_y\}^T$ along parts of the boundary ∂S of S has the same effect as constraining the stiffness matrices obtained by the right hand side of Lemma 3.1 by using the boundary conditions $\{\tilde{u}_x \circ \varphi^\beta, \tilde{u}_y \circ \varphi^\beta\}^T$ along the corresponding boundaries of S^*.

4 The Method of Auxiliary Mapping: A New Approach to Deal with Singularities

4.1 Description and Implementation of the Method

Overall structure of our method is as follows. From the arguments given in section 2.1, if no body forces are present, then in a neighborhood S_P of a singular point P, each

component of the displacement vector can be written as

$$u_P(r, \theta) = \sum_{j=1}^{Q(P)} K_j F_j(r) G_j(\theta) + w_{Q(P)}(r, \theta). \tag{30}$$

Here (r, θ) are the polar coordinates with respect to the singular point P. The function $G_j(\theta)$ is analytic up to the boundary of S_P and $F_j(r) = Re(r^{\lambda_{P_j}} \log^\rho(r))$ or $Im(r^{\lambda_{P_j}} \log^\rho(r))$, where $\rho = 0$ except for some special angles. The eigenvalues λ_{P_j} are in general complex numbers with positive real parts and $Re(\lambda_{P_j}) \leq Re(\lambda_{P_{j+1}})$. $F_j(r), G_j(\theta)$ depend on the interior (wedge) angle α; K_j are stress intensity factors. $w_{Q(P)}$ is smoother than the first term on the right hand side of (30). $Q(P)$ is a positive integer and $Re(\lambda_{PQ(P)}) < 1$. Let $\lambda_{P_1}^{(r)}$ be the smallest real number of $Re(\lambda_{P_j})$ and suppose $\lambda_{P_1}^{(r)} < 1$. If we let $\beta = 1/\lambda_{P_1}^{(r)}$ and (r^*, θ^*) denotes the polar coordinate system on S_P^* centered at P^*, then

$$\hat{u}_P(r^*, \theta^*) = \sum_{j=1}^{Q(P)} K_j F_j((r^*)^\beta) G_j(\beta \theta^*) + w_{Q(P)}((r^*)^\beta, \beta \theta^*) \tag{31}$$

and $\beta \lambda_{P_j}^{(r)} \geq 1$ for $j = 1, ..., Q(P)$. Therefore $\hat{u}_P(r^*, \theta^*) = (u_P \circ \varphi^\beta)(r^*, \theta^*)$ is in $H^m(S_P^*), m > 2$.

Thus, on S_P^*, the standard finite element method could yield a good approximation of $\hat{u}_P$ in $H^1(S_P^*)$. Since our auxiliary mappings are conforming and the mapping sizes β are assumed to be > 1, the H^1-norm is preserved under the transformation by the auxiliary mapping. Thus, approximating $\hat{u}_P$ in $H^1(S_P^*)$ by the standard finite element basis functions defined on S_P^* has the same effect as approximating u_P on S_P in $H^1(S_P)$ by using singular basis functions on S_P constructed through the auxiliary mapping φ^β. However, the novelty of our method lies in never constructing such singular basis functions.

We now describe our method, the *Method of Auxiliary Mapping* (MAM). Suppose the exact solution $\{u\}$ has singularities at $P_1, P_2, ..., P_M$. In what follows, u denotes the displacements u_x and u_y. In this case, our method goes as follows:

Step 1: Determination of the Singular Regions

At each singular point P_q, construct a neighborhood of the singular point P_q, a sector S_q centered at P_q. Namely,

$$S_q = \{(r, \theta) : 0 \leq r \leq R_q\} \cap \Omega,$$

where (r, θ) are the polar coordinates at P_q. Our method is not sensitive to the size of the radius R_q, provided R_q is chosen small enough so that S_q is a circular sector in Ω and any two different neighborhoods of two singularities are disjoint. R_q is usually selected to be ≤ 1.

Step 2: Selection of Auxiliary Mappings

Suppose $\lambda_{q1}^{(r)}$ is $\min\{Re(\lambda_{qj})\}$, where λ_{qj} are the eigenvalues of the singularity at P_q. Then *the mapping sizes* of auxiliary mappings are selected as follows:

$$\beta_q = \begin{cases} \dfrac{1}{\lambda_{q1}^{(r)}}, & \text{if } \lambda_{q1}^{(r)} < 1, \\ 1, & \text{otherwise.} \end{cases} \tag{32}$$

Now the auxiliary mapping $\varphi^{\beta_q} : S_q^* \to S_q$ is defined by $z = \varphi^{\beta_q}(\zeta) = \zeta^{\beta_q}$, a conformal mapping from the ζ-plane to the z-plane.

Step 3: Triangulation of Ω

For each S_q , generate a curvilinear triangulation $\mathcal{T}_q$ of S_q as shown in Fig. 4.1. Then construct a triangulation $\mathcal{T}$ on Ω such that $\mathcal{T}|_{S_q} = \mathcal{T}_q$. Let $\mathcal{T}_q^*$ be the image of $\mathcal{T}_q$ under $(\varphi^{\beta_q})^{-1}$ (see, Fig. 4.1).

For $e^* \in \mathcal{T}_q^*$ ($e \in \mathcal{T}_0 = \mathcal{T}\backslash \cup \mathcal{T}_q$), Φ_{e^*} (Φ_e) is the usual elemental mapping from the standard element Ω_{st} (which is either the reference triangle or rectangle depending on whether e^* (e) is a triangular or a rectangular element) onto curvilinear elements $e^*(e)$ respectively. Since we allow circular arcs as sides of elements, the elemental mappings could be of the *blending type*([14]) as those in chapter 6 of ([36]) and satisfy the usual technical conditions([4],[20]) that lead to conforming finite elements.

Step 4: Computation of Stiffness Matrix and Load Vector.

In computing local stiffness matrices and local load vectors,

- Use the standard elemental mapping Φ_e for the elements e in the nonsingular region $\Omega_0 = \Omega\backslash \cup_{q=1}^M S_q$.

- Use the standard elemental mappings Φ_{e^*} for the elements e in the singular regions $\cup_{q=1}^M S_q$; in other words, local stiffness matrices and load vectors on the element e in the singular region are replaced by those computed on the elements $e_* = (\varphi^\beta)^{-1}(e)$ by using the right hand sides of equations (28) and (29).

Let Φ_e^S denote the special elemental mapping from Ω_{st} onto $e \in \mathcal{T}_q$ defined by $\Phi_e^S = \varphi^{\beta_q} \circ \Phi_{e^*}$. We will call this special elemental mapping Φ_e^S *the singular elemental mapping*.

Remark 4.1. (1) If Φ_e^S is used as the elemental mapping on the element e in a singular region S_q then the basis functions constructed through Φ_e^S will mimic the original singularity on S_q.

(2) Suppose $e_1 \in \mathcal{T}_0$, $e_2 \in \cup \mathcal{T}_q$ and $\gamma = e_1 \cap e_2 = \{(r_0, \theta) : a \leq \theta \leq b\}$. Then the conformal mapping $(\varphi^{\beta_q})^{-1}$ is linear on the closed interval $[a, b]$; therefore, the basis functions constructed by using the usual elemental mapping Φ_e for $e \subset \Omega_0$ and the singular elemental mapping Φ_e^S for $e \subset \cup S_q$ are continuous along their common edges.

Let $\bar{\mathcal{N}}_j$ be the standard shape functions on Ω_{st}, $\mathcal{N}_j^* = \bar{\mathcal{N}}_j \circ \Phi_{e^*}^{-1}$ and $\mathcal{N}_j = \bar{\mathcal{N}}_j \circ (\Phi_e^S)^{-1}$. Then $\mathcal{N}_j \circ \varphi^\beta = \mathcal{N}_j^*$. Hence, from Lemma 2.1 , we have

$$\iint_e \nabla \mathcal{N}_i [a_{ij}](\nabla \mathcal{N}_j)^T dx = \iint_{e^*} \nabla \mathcal{N}_i^* [q_{ij}](\nabla \mathcal{N}_j^*)^T d\xi \tag{33}$$

$$\iint_e f \mathcal{N}_j dx = \iint_{e^*} |J(\varphi^\beta)| \hat{f} \mathcal{N}_j^* d\xi. \tag{34}$$

Instead of computing the left-hand sides of (33)-(34) involving singular shape functions, we compute the right-hand sides of the equations for the local stiffness matrix and load vector on the elements e in the singular regions. Let us note that from Lemma 3.1 the coefficient q_{ij} are not singular. Moreover, If β is chosen to be an integer > 2, the integrand of the left hand side of (34) is as smooth as f.

Thus, the computer implementation of our method is quite simple since any existing finite element code can be used for the computation of the right-hand sides without any alterations. Indeed, in MAM, unlike other singular function approaches, the banded structure of the resulting stiffness matrix is not lost and no severe problem with ill conditioning will occur.
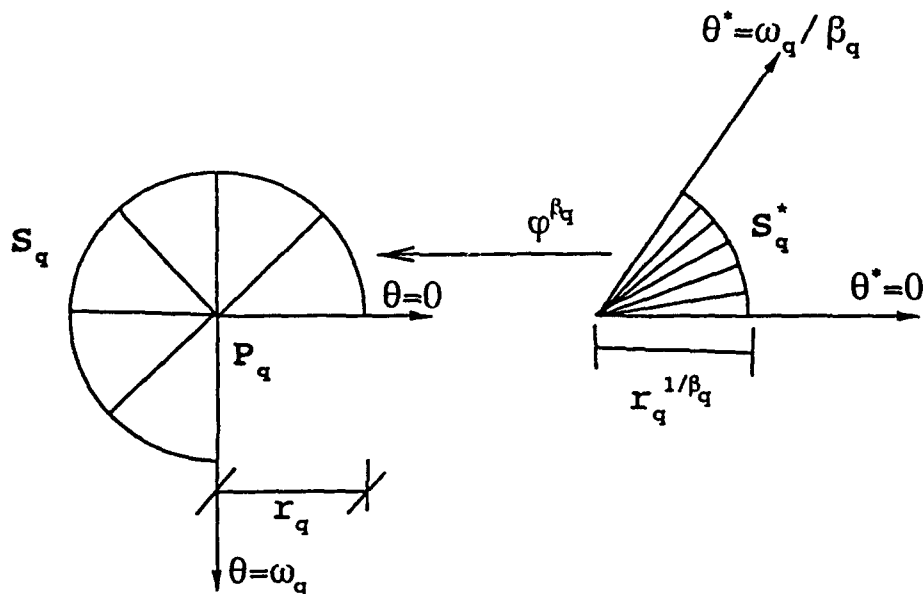

Fig. 4.1. A singular neighborhood S_q of a singular point P_q and its mapped domain S_q^* under the mapping φ^{β_q}. The scheme $\mathcal{T}_q^*$ on S_q^* and the corresponding mesh $\mathcal{T}_q$ on S_q.

Let $V_p = \{\{w\} = (w_1, w_2) \in H_D^1(\Omega) : w_i|_e \circ \Phi_e(w_i|_e \circ \Phi_e^S)$ is a polynomial of degree p on Ω_{st} for all elements e in Ω_0 (e in $\cup_{q=1}^M S_q$)$\}$, where Ω_{st} is the standard triangle, T, or the standard rectangle, Q, according to whether e is a triangular element or a rectangular element. Then **the p-version of the Finite Element Method** in our context is as follows: Find an element $\{u_p\} \in V_p$ such that

$$\mathcal{B}(\{u_p\}, \{v\}) = \mathcal{F}(\{v\}), \text{ for all } \{v\} \in V_p. \tag{35}$$

The dimension of V_p will be denoted by N_p and will be called the degree of freedom(**DOF**). Let us note that in the p-version of the finite element method the triangulation of Ω is fixed and only the degree p of the basis polynomials is increased.

If $\{u_{ex}\}$ is the solution of (6) then

$$\|\{u_p\} - \{u_{ex}\}\|_E = \min_{\{w\} \in V_p} \|\{w\} - \{u_{ex}\}\|_E, \tag{36}$$

where $\|\{w\}\|_E^2 = \dfrac{1}{2}\mathcal{B}(\{w\}, \{w\})$ is the energy norm.

4.2　The Rate of Convergence.

Let Ω_0 and S_q be the same as those in the preceding argument. Suppose $u_{ex}|_{\Omega_0} \in H^{\nu_0}(\Omega_0), u_{ex}|_{S_q} \in H^{\nu_q}(S_q)$, $\nu_0 \geq 2$, $\nu_q < 2$, $1 \leq q \leq M$, and if $\lambda_{q1}^{(r)} = \min\{Re(\lambda_{qj})\} < 1$, then our method with auxiliary mapping $\varphi^{\beta_q}, \beta_q = 1/\lambda_{q1}^{(r)}$ will greatly reduce the intensity of the singularity at P_q. Therefore, $\hat{u}_{ex} = u_{ex}|_{S_q} \circ \varphi^{\beta_q} \in H^{\nu_q^*}(S_q^*)$ and $\nu_q^* > 2$, which is larger than ν_q.

By using the inequality (see [30] for detail),

$$\|v\|_{1,S} \leq \|\hat{v}\|_{1,S^*},$$

the following theorem was proved in ([30]).

Theorem 3.1. *Suppose $u_p^{(\beta_1, \cdots, \beta_M)}$ is the finite element solution, on a quasi uniform mesh, obtained by employing the method of auxiliary mapping with the auxiliary mapping φ^{β_q} on each singular region S_q in the framework of the p-version of the finite element method. Then we have*

$$\|u_p^{(\beta_1, \cdots, \beta_M)} - u_{ex}\|_{1,\Omega} \leq \left[C_0 \frac{\|u_{ex}\|_{\nu_0,\Omega_0}}{N_p^{(\nu_0-1)/2}} + \sum_{q=1}^M C_q \frac{\|\hat{u}_{ex}\|_{\nu_q^*,S_q^*}}{N_p^{(\nu_q^*-1)/2}} \right] \tag{37}$$

where N_p is the degree of freedom and, for each q, $0 \leq q \leq M$, C_q is independent of N_p.

13

4.3 Computation of Strains and Stress

The strains are computed from the strain-displacement relationships and the stresses are computed directly from the strain-stress relationships. However, in MAM, those computations on the singular regions are different from the standard approach.

(4.3A). Suppose ψ is the inverse mapping of the auxiliary mapping $\varphi^\beta : S^* \to S$, defined by (26), and $J(\varphi^\beta) = \partial(x_1, x_2)/\partial(\xi_1, \xi_2)$ denotes the Jacobian matrix of φ^β. Then $\left[J(\psi) \circ \varphi^\beta \right] \cdot J(\varphi^\beta) = I$ and hence

$$[J(\varphi)]^{-1} = J(\psi) \circ \varphi^\beta. \tag{38}$$

Moreover,

$$
\begin{aligned}
\widehat{J(\psi)} &= J(\psi) \circ \varphi^\beta \\
&= \frac{1}{\beta}(r)^{(1-\beta)/\beta}
\begin{bmatrix}
\cos(\frac{1-\beta}{\beta})\theta & -\sin(\frac{1-\beta}{\beta})\theta \\
\sin(\frac{1-\beta}{\beta})\theta & \cos(\frac{1-\beta}{\beta})\theta
\end{bmatrix}
\circ \varphi^\beta \\
&= \frac{1}{\beta}(r^*)^{1-\beta}
\begin{bmatrix}
\cos(1-\beta)\theta^* & -\sin(1-\beta)\theta^* \\
\sin(1-\beta)\theta^* & \cos(1-\beta)\theta^*
\end{bmatrix}.
\end{aligned}
\tag{39}
$$

Let us recall the singular elemental mapping for an element e is defined by

$$\Phi^S = \varphi \circ \Phi : E \to e,$$

where $\varphi : e^* \to e$ is the auxiliary mapping defined by $z = \xi^\beta$ and $\Phi : E \to e^*$ is the standard elemental mapping. Now we have

$$
\begin{aligned}
\left[J(\Phi^S) \right]^{-1} &= [J(\varphi \circ \Phi)]^{-1} \\
&= J([\varphi \circ \Phi]^{-1}) \circ (\varphi \circ \Phi) \\
&= \left[J(\Phi^{-1} \circ \varphi^{-1}) \right] \circ (\varphi \circ \Phi) \\
&= \left[(J(\Phi^{-1}) \circ \varphi^{-1}) \cdot J(\varphi^{-1}) \right] \circ (\varphi \circ \Phi) \\
&= \{ (([J(\Phi)]^{-1} \circ \Phi^{-1}) \circ \varphi^{-1}) \cdot \\
&\qquad ([J(\varphi)]^{-1} \circ \varphi^{-1}) \} \circ (\varphi \circ \Phi) \text{ by (38)} \\
&= ([J(\Phi)]^{-1}) \cdot ([J(\varphi)]^{-1} \circ \Phi)
\end{aligned}
$$

and hence

$$
\begin{aligned}
\left[J(\Phi^S)^T \right]^{-1} &= ([J(\varphi)]^{-1} \circ \Phi)^T \cdot ([J(\Phi)]^{-1})^T \\
&= ([J(\varphi)]^{-1} \circ \Phi)^T \cdot ([J(\Phi)]^T)^{-1}.
\end{aligned}
\tag{40}
$$

Suppose $P = (x_1, x_2)$ is a point in an element $e \subset \Omega$ and let $\Phi : E \to e$ be the elemental mapping. Then the strains at P are

$$\{\epsilon_x^{(u)}, \epsilon_y^{(u)}, \gamma_{xy}^{(u)}\}^T(P) = [D]\{u_1, u_2\}(P)$$

$$= \begin{bmatrix} 1 & 0 \\ 0 & 0 \\ 0 & 1 \end{bmatrix} \nabla_x u_1(P) + \begin{bmatrix} 0 & 0 \\ 0 & 1 \\ 1 & 0 \end{bmatrix} \nabla_x u_2(P)$$

$$= \begin{bmatrix} 1 & 0 \\ 0 & 0 \\ 0 & 1 \end{bmatrix} \left[J(\Phi)^T\right]^{-1}(\bar{P}) \sum_{I=1}^n a_I \nabla_\xi \mathcal{N}_I(\bar{P})$$

$$+ \begin{bmatrix} 0 & 0 \\ 0 & 1 \\ 1 & 0 \end{bmatrix} \left[J(\Phi)^T\right]^{-1}(\bar{P}) \sum_{I=1}^n a_{I+n} \nabla_\xi \mathcal{N}_I(\bar{P}),$$

where $\Phi(\bar{P}) = P$, $\nabla_x = (\frac{\partial}{\partial x_1}, \frac{\partial}{\partial x_2})^T$ and $\nabla_\xi = (\frac{\partial}{\partial \xi_1}, \frac{\partial}{\partial \xi_2})^T$.

Suppose e is an element in the singular region on which MAM is applied, then $\left[J(\Phi)^T\right]^{-1}$ is replaced by $\left[J(\Phi^S)^T\right]^{-1}$ and it follows from (39) and (40) that

$$\left[J(\Phi^S)^T\right]^{-1} = ([J(\varphi)]^{-1} \circ \Phi)^T \cdot ([J(\Phi)]^{-1})^T$$

$$= \frac{1}{\beta}(r^*)^{1-\beta} \begin{bmatrix} \cos(1-\beta)\theta^* & -\sin(1-\beta)\theta^* \\ \sin(1-\beta)\theta^* & \cos(1-\beta)\theta^* \end{bmatrix} \cdot \begin{bmatrix} J_{11}^* & J_{12}^* \\ J_{21}^* & J_{22}^* \end{bmatrix}, \quad (41)$$

where J_{ij}^* is the (i,j) component of $([J(\Phi)]^T)^{-1}$.

It should be noted that in (41), the exponent $(1 - \beta) < 0$ since the mapping size β is larger than 1. Thus, unlike the standard finite element solution, from (41), we can see that the strains at the singular points, calculated from the finite element solution obtained by using MAM, are infinity. This is because our solution by MAM resembles the exact solution near the singularities.

(4.3B) The stresses are computed from the stress-strain relation. Usually the principal stress and the equivalent stress are of engineering interest. The eigenvalues of the following matrix

$$\begin{bmatrix} \sigma_{11} & \sigma_{12} \\ \sigma_{11} & \sigma_{12} \end{bmatrix}$$

are called the principal stresses and they will be denoted by $\sigma_{(1)}$ and $\sigma_{(2)}$. The lines which are perpendicular to the eigenvectors of this matrix are called the principal lines.

In the case of plane stress, the third principal stress $\sigma_{(3)} = 0$ and in the case of plane strain, $\sigma_{(3)} = \nu(\sigma_{(1)} + \sigma_{(2)})$. Now the equivalent stress is defined as follows:

$$\sigma_e^2 = \frac{1}{2}\left[(\sigma_{(1)} - \sigma_{(2)})^2 + (\sigma_{(2)} - \sigma_{(3)})^2 + (\sigma_{(3)} - \sigma_{(1)})^2\right].$$

15

5 Numerical Results

In [28] and [30] some comparisons were made between MAM (the Method of Auxiliary Mapping) and some of the best of alternative methods such as Finite Difference, Finite Element, and singular function methods. As benchmarks, elliptic problems having corner, jump boundary data, or interface singularity were considered. In comparisons given there, it was shown that MAM virtually requires no extra cost. Since CPU time comparisons for elasticity problems between MAM and alternative approaches are essentially the same as those in the previous papers, we only compare accuracy versus DOF(Degree of Freedom) between MAM and the conventional approach in the framework of the p-version of the Finite Element Method.

In the first two examples, the performance of the Method of Auxiliary Mapping in the framework of the p-version of the Finite Element Method will be tested using the elasticity problems whose true solutions are known. In this section, all computations are the plane stress. Recall the auxiliary mapping is defined by

$$\varphi^\beta(r,\theta) = (r^\beta \cos(\beta\theta), r^\beta \sin(\beta\theta)) \tag{42}$$

The number β is called *the mapping size* of the auxiliary mapping. Throughout this section, " With Map " stands for the results obtained by applying MAM on Mesh I(the initial coarse mesh), shown in Fig. 5.1. " No Map " stands for the results obtained by the standard Finite Element Method on Mesh I without applying MAM.

Example 5.I. Suppose the tractions are free along the boundaries $\alpha = \pm\pi$ in Fig. 3.1. Then by using a similar argument given in §3.1, the smallest eigenvalue is $\lambda = 0.5$ and the corresponding stress functions are

$$
\begin{aligned}
\sigma_x &= \lambda r^{(\lambda-1)}\{(2 - Q(\lambda+1))\cos((\lambda-1)\theta) \\
&\qquad -(\lambda-1)\cos((\lambda-3)\theta)\} \tag{43}
\end{aligned}
$$

$$
\begin{aligned}
\sigma_y &= \lambda r^{(\lambda-1)}\{(2 + Q(\lambda+1))\cos((\lambda-1)\theta) \\
&\qquad +(\lambda-1)\cos((\lambda-3)\theta)\} \tag{44}
\end{aligned}
$$

$$
\begin{aligned}
\tau_{xy} &= \lambda r^{(\lambda-1)}\{(\lambda-1)\sin((\lambda-3)\theta) \\
&\qquad +Q(\lambda+1)\sin((\lambda-1)\theta)\}, \tag{45}
\end{aligned}
$$

where $\lambda = 0.5$ and $Q = 1/3$.

Let us consider the equations of elasticity on a domain $\Omega_1 = \{(x,y) : -2 \leq x \leq 2, -2 \leq y \leq 2\}$ shown in Fig. 5.1, with crack along the negative x-axis, which is isotropic with material constants $E = 1000$(modulus of elasticity) and $\nu = 0.3$ (Poisson's ratio).

The traction functions given by (43)-(45) are imposed along the entire boundary of Ω_1, including both sides of the crack. Furthermore, the following constraints are imposed: the displacement vector at $(0,0)$ is fixed and the y-components of the displacement vector at $(2,0)$ is fixed.

16

On the mesh shown in Fig. 5.1, MAM is applied with mapping size $\beta = 4$. In order to show the effectiveness of MAM, the true stress, the computed stress obtained by using MAM, and the computed stress by the standard Finite Element Method are compared one another. In Fig. 5.2, the stress σ_y on $[0,1] \times [-\pi, \pi]$ are compared. In Fig. 5.3, the shear stress τ_{xy} are compared on the same subregion. From Fig. 5.2 and Fig. 5.3, one can see that MAM is quite effective in handling crack singularity. In other words, one can not see any difference between the true stress and the computed stress obtained by using MAM. However, there is significant difference between the true stress and the computed stress by the standard FEM. The stress tensor along the line $y = 0.0129$ are given in Table 5.1.

The crack singularity discussed in Example 5.I is not too strong. Thus it is possible to obtain a practical solution by sufficiently refining the mesh on the domain Ω_1. However, as mentioned in §3.1, there are some elasticity problems containing singularities which are too strong for the mesh refinement method to yield any practical solutions.

In the next example, it will be shown that MAM can give an accurate solution even for those problems to which the mesh refinement method alone can not yield any practical solutions.
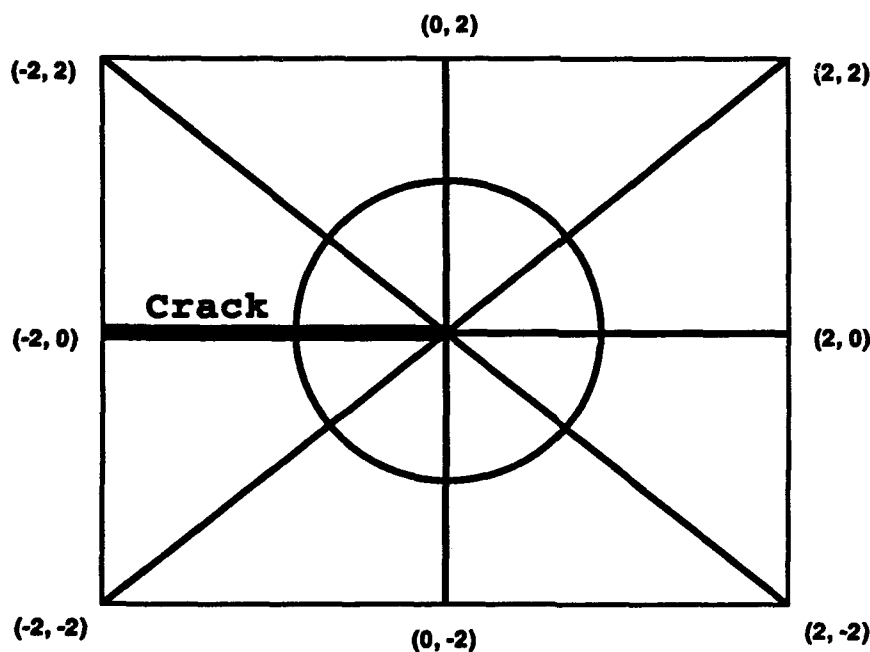

Fig. 5.1. The scheme of the domain Ω_1 and Mesh I.

17

Table 5.1. The Stress $\sigma_x, \sigma_y, \tau_{xy}$ along the line $y = 0.0129$: True(True stress), With No Map(computed Stress by the standard FEM) and With Map (computed Stress by using MAM). The computed stresses are obtained by using basis functions of order 8.

x	y	σ_x True	σ_x No Map	σ_x With Map
-0.40000	0.0129	0.05093822	0.04823590	0.05089369
-0.34839	0.0129	0.06264135	0.15461398	0.06262561
-0.29677	0.0129	0.07962216	0.22911948	0.07964541
-0.24516	0.0129	0.10593000	0.20079910	0.10599321
-0.19355	0.0129	0.15069789	0.05516336	0.15078407
-0.14194	0.0129	0.23883382	-0.05363119	0.23890443
-0.09032	0.0129	0.46349907	0.37045664	0.46355612
-0.03871	0.0129	1.48632567	2.41385925	1.48644065
-0.01290	0.0129	3.83449701	4.62512498	3.83435649
0.01290	0.0129	4.42121220	5.63512478	4.42443179
0.03871	0.0129	4.52331891	4.53508576	4.52399697
0.09032	0.0129	3.25283283	3.16439666	3.25273651
0.14194	0.0129	2.62989437	2.47764699	2.62995116
0.19355	0.0129	2.26172620	2.13848521	2.26183925
0.24516	0.0129	2.01336763	1.95231425	2.01344754
0.40000	0.0129	1.57929020	1.58108784	1.57924127

| σ_y True	σ_y No Map	σ_y With Map	σ_{xy} True	σ_{xy} No Map	σ_{xy} With Map
0.00003312	-0.02967877	-0.00014424	-0.00123211	0.00510379	-0.00123076
0.00005368	0.03406785	-0.00003871	-0.00173954	-0.07977106	-0.00176440
0.00009401	0.09624285	0.00012811	-0.00259535	-0.13304302	-0.00265020
0.00018323	0.08994510	0.00034680	-0.00417904	-0.08602245	-0.00426194
0.00041800	-0.03752552	0.00063424	-0.00752793	0.08568925	-0.00762896
0.00123034	-0.23020095	0.00132026	-0.01625616	0.26892630	-0.01635764
0.00587308	-0.15340532	0.00583234	-0.04945086	0.07111119	-0.04952390
0.09964524	1.07899882	0.10064434	-0.36327765	-1.38006892	-0.36333288
1.83132606	2.65316096	1.83542437	-2.41804125	-3.04412791	-2.41681990
9.25729470	6.04753022	9.25774822	1.00158548	1.19976481	1.00025011
5.24987421	4.78600541	5.25097506	0.69334021	0.73212362	0.69287164
3.35173455	3.25907239	3.35178881	0.22881300	0.22695570	0.22885594
2.66240669	2.52571398	2.66266548	0.11880174	0.05174389	0.11869870
2.27678206	2.17434706	2.27711095	0.07513994	0.02115217	0.07496224
2.02172571	1.97913221	2.02198072	0.05287338	0.03560597	0.05272972
1.58175442	1.57152579	1.58166512	0.02545255	0.04008938	0.02552800
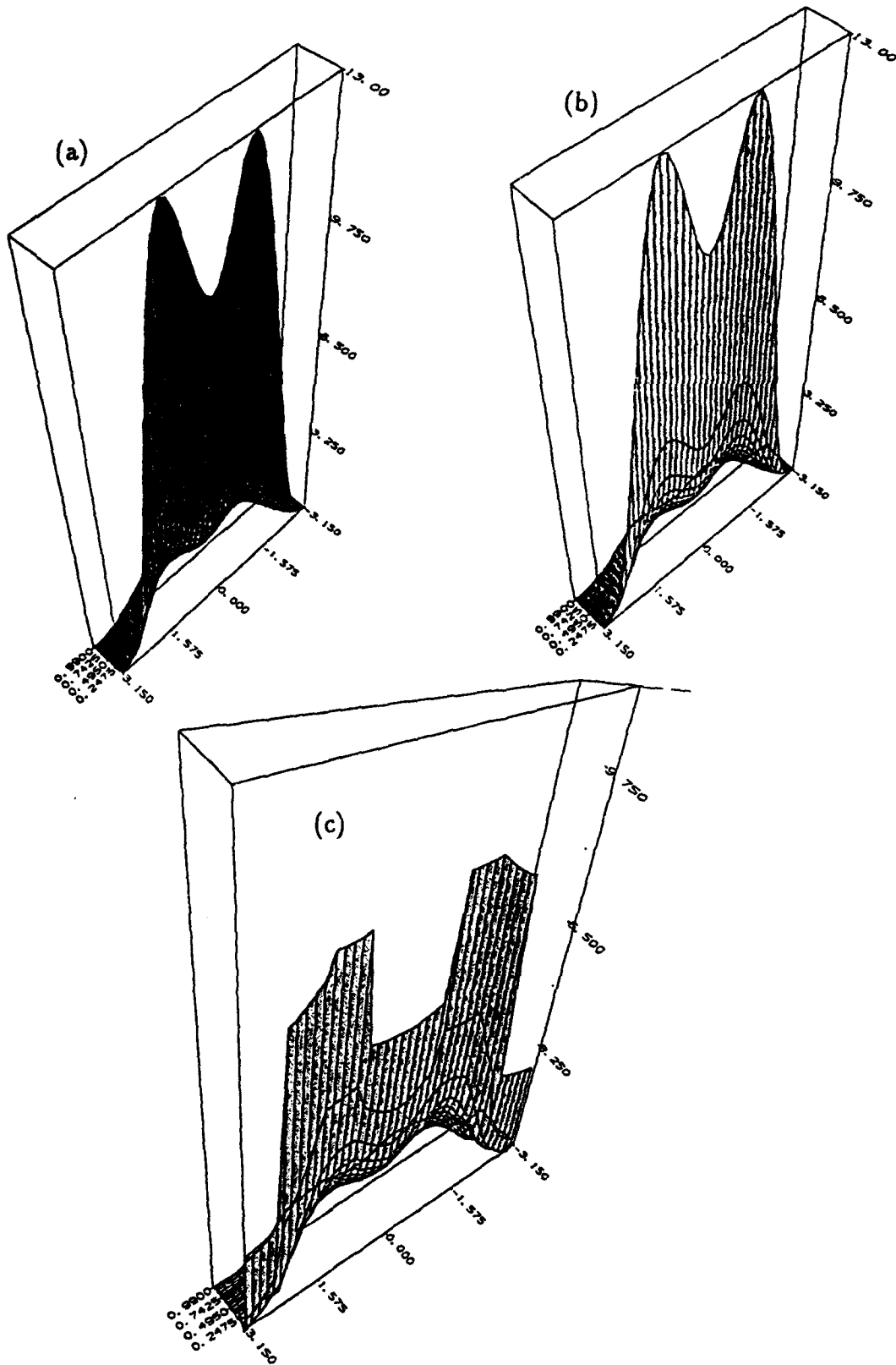
Fig. 5.2. The stress σ_x on $[0,1] \times [-\pi, \pi]$: (a) True stress, (b) computed stress by MAM, and (c) computed stress without using MAM. In cases (b) and (c), the number of degrees of freedom are the same and basis functions of order 8 are used.
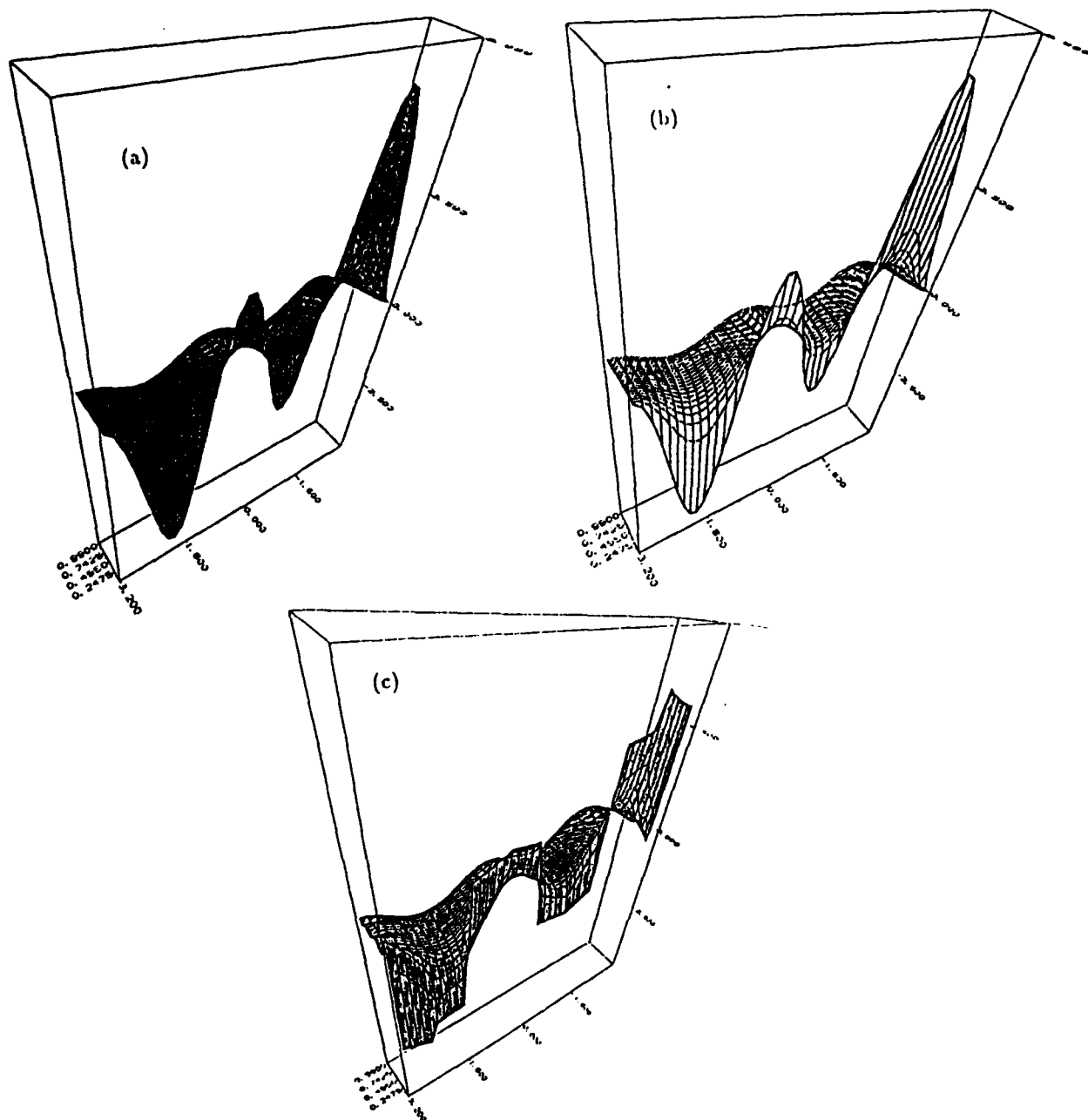
Fig. 5.3. The stress τ_{xy} on $[0,1] \times [-\pi, \pi]$: (a) True stress, (b) computed stress by using MAM, and (c) computed stress without using MAM. In cases (b) and (c), the number of degrees of freedom are the same and basis functions of order 8 are used.

Although this paper is concerned with the equations of elasticity on polygonal domains, for brevity, we consider an elasticity problem on a sector region in the next example.

Example 5.II. Consider the equations of elasticity (11) and (12) in a wedge-shaped domain

$$\Omega_2^{(\pm\alpha)} = \{(r,\theta) : r \leq 2, -\alpha \leq \theta \leq \alpha\}, 0 \leq \alpha \leq 90°$$

which is isotropic with material constants $E = 1000$ and $\nu = 0.3$. The displacement functions given below satisfy the equations of elasticity in the domain $\Omega_2^{(\pm\alpha)}$:

$$u_r(r,\theta) = \frac{r^\lambda}{2G}\{-(\lambda+1)f(\theta)\} \tag{46}$$

$$u_\theta(r,\theta) = \frac{r^\lambda}{2G}\{-f'(\theta)\}, \tag{47}$$

where

$$f(\theta) = \sin(\lambda+1)\theta$$
$$\lambda = \frac{90°}{\alpha} - 1$$
$$G = \frac{E}{2(1+\nu)}.$$

The corresponding stress tensor are

$$\sigma_r = r^{(\lambda-1)}\{(\lambda+1) - (\lambda+1)^2\}\sin(\lambda+1)\theta,$$
$$\sigma_\theta = r^{(\lambda-1)}\lambda(\lambda+1)\sin(\lambda+1)\theta,$$
$$\tau_{r\theta} = -r^{\lambda-1}\lambda(\lambda+1)\cos(\lambda+1)\theta.$$

It is worth noting that $u_\theta = \tau_{r\theta} = 0$ along the boundary $\theta = \pm\alpha$. Thus this problem could be solved so that the condition $u_\theta = 0$ would be imposed by proper combination of u_x and u_y. Nevertheless, here we will impose the displacements(nonhomogeneous essential boundary conditions) along the entire boundary of the domain. Let us note that the displacements are strongly singular at the vertex. In this example we show that our method performs very well even for this case. In the p-version of Finite Element Method, used for this example, the essential boundary conditions are imposed by the L_2 projection. Hence the error of the method now includes also the error of the approximation of the boundary condition. Therefore, we have to expect that the strain energy will not necessarily be monotonically decreasing with p, the order of base functions, as it would be if the nonhomogeneous boundary condition would be satisfied exactly (See also remark 5.1). Let us note that in all other examples mentioned in this paper natural boundary conditions are used; hence the strain energy is monotonically increasing with p.

Let $\Omega_2^{(\alpha)}$ be the upper half of $\Omega_2^{(\pm\alpha)}$ as shown in Fig 5.4. Along the entire boundary of $\Omega_2^{(\alpha)}$, the following displacement functions in the x-y coordinate system are imposed:

$$u_x = u_r \cos\theta - u_\theta \sin\theta$$
$$u_y = u_r \sin\theta + u_\theta \cos\theta$$

which correspond to the displacement functions (46) and (47) in the polar coordinate system. The singularity of this problem can be as strong as desired by taking α close to 90° as shown in Fig. 3.2 and Table 5.2.

Furthermore, it is not difficult to show that

$$\frac{\partial u_x}{\partial x} = A\lambda r^{(\lambda-1)} \sin(\lambda-1)\theta,$$

$$\frac{\partial u_x}{\partial y} = A\lambda r^{(\lambda-1)} \cos(\lambda-1)\theta,$$

$$\frac{\partial v_x}{\partial x} = A\lambda r^{(\lambda-1)} \cos(\lambda-1)\theta,$$

$$\frac{\partial v_x}{\partial y} = -A\lambda r^{(\lambda-1)} \sin(\lambda-1)\theta,$$

where $A = -(\lambda+1)/(2G)$. Thus, for six representative wedge angles $\alpha = 50°, 60°, 70°, 80°, 85°, 89°$, the true strain energy $(1/2)\mathcal{B}(\{u_{ex}\}, \{u_{ex}\}), \{u_{ex}\} = \{u_x, u_y\}^T$, on the domain $\Omega_2^{(\alpha)}$ are as follows:

On $\Omega_2^{(50)}$, $\quad \mathcal{U}(\{u_{ex}\}) = 0.44570111132335915$D-02

On $\Omega_2^{(60)}$, $\quad \mathcal{U}(\{u_{ex}\}) = 0.15315264186250224$D-02

On $\Omega_2^{(70)}$, $\quad \mathcal{U}(\{u_{ex}\}) = 0.55734845185448461$D-03

On $\Omega_2^{(80)}$, $\quad \mathcal{U}(\{u_{ex}\}) = 0.17074707317282833$D-03

On $\Omega_2^{(85)}$, $\quad \mathcal{U}(\{u_{ex}\}) = 0.68995884499654107$D-04

On $\Omega_2^{(89)}$, $\quad \mathcal{U}(\{u_{ex}\}) = 0.11783124402203123$D-04.

Now $\Omega_S^{(\alpha)} = \{(r,\theta) : r \leq 1, 0 \leq \theta \leq \alpha\} \subset \Omega_2^{(\alpha)}$ is chosen as a singular region, a neighborhood of the singular point $(0,0)$, on which MAM will be applied. As it was mentioned in Remark 3.2,

$$u_x \circ \varphi^\beta \text{ and } u_y \circ \varphi^\beta$$

are imposed along the boundaries $\theta^* = 0$ and $\theta^* = \dfrac{\alpha}{\beta}$ of $(\Omega_S^{(\alpha)})^* = \{(r^*, \theta^*) : r^* \leq 1, \theta^* \leq \alpha/\beta\}$. Here β is an optimal mapping size, $1/\lambda = \alpha/(90-\alpha)$.

Table 5.2. The eigenvalue $\lambda = 90°/\alpha - 1$ for six representative wedge angles α.

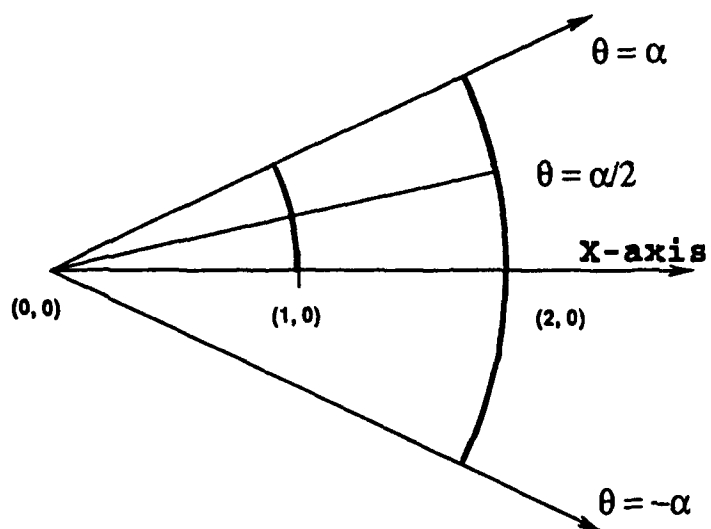| α	50°	60°	70°	80°	85°	89°
λ	0.80000	0.50000	0.286714	0.125	0.0588235	0.01124

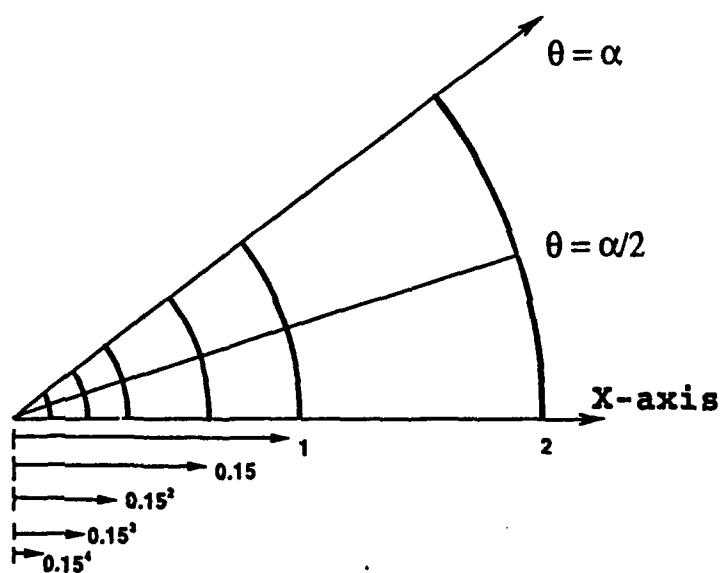**Fig. 5.4.** The scheme of Mesh I on the domain $\Omega_2^{(\pm\alpha)}$.

Fig. 5.5. The scheme of Mesh V on the domain $\Omega_2^{(\alpha)}$.

Table 5.3. The strain energies on the domain $\Omega_2^{(\alpha)}$ for $\alpha = 50°, 60°, 70°, 80°, 85°, 89°$ when MAM is applied.

p-deg	DOF	50°	60°	70°
1	2	0.4387492745431457D-02	0.15209859482894121D-02	0.55673457293105253D-03
2	10	0.4456887439527751D-02	0.1531572785147233D-02	0.5573874898294548D-03
3	22	0.4457011922197191D-02	0.1531527952481516D-02	0.5573494680021682D-03
4	42	0.4457011143393066D-02	0.1531526450827115D-02	0.5573484777837966D-03
5	70	0.4457011132531040D-02	0.1531526419381477D-02	0.5573484525381751D-03
6	106	0.4457011132340058D-02	0.1531526418643714D-02	0.5573484518728477D-03
7	150	0.4457011132336056D-02	0.1531526418625500D-02	0.5573484518549730D-03
8	202	0.4457011132335964D-02	0.1531526418625041D-02	0.5573484518544919D-03

p-deg	DOF	80°	85°	89°
1	2	0.1709561207603345D-03	0.6906812121402299D-04	0.11786395375517020D-04
2	10	0.1707578614952583D-03	0.6899855353039026D-04	0.1178322837770610D-04
3	22	0.1707473741570929D-03	0.6899596270247496D-04	0.1178312715834583D-04
4	42	0.1707470816190254D-03	0.6899588725323426D-04	0.1178312411538886D-04
5	70	0.1707470734116305D-03	0.6899588506198350D-04	0.1178312402485034D-04
6	106	0.1707470731796349D-03	0.6899588499832774D-04	0.1178312402218292D-04
7	150	0.1707470731730394D-03	0.6899588499647640D-04	0.1178312402211005D-04
8	202	0.1707470731728518D-03	0.6899588499642211D-04	0.1178312402209949D-04

Table 5.4. The strain energy on the domain $\Omega_2^{(\alpha)}$ obtained by the optimal mesh refinement, Mesh V.

p-deg	DOF	50°	60°	70°
1	10	0.4405670020540130D-02	0.1566487115006998D-02	0.6053103198646025D-03
2	42	0.4457420260186373D-02	0.1534472170765279D-02	0.5647415490783892D-03
3	78	0.4457064766350695D-02	0.1531924078512398D-02	0.5606895925910377D-03
4	138	0.4457017168219616D-02	0.1531597705602884D-02	0.5597224836509342D-03
5	222	0.4457011931428601D-02	0.1531546547014034D-02	0.5591135803203382D-03
6	330	0.4457011249115450D-02	0.1531535988017260D-02	0.5587320835784172D-03
7	462	0.4457011150167903D-02	0.1531531515488644D-02	0.5582545129703971D-03
8	618	0.4457011135802711D-02	0.1531529449633110D-02	0.5579538617159367D-03

p-deg	DOF	80°	85°	89°
1	10	0.2889017640162947D-03	0.3576618879140340D-03	0.6182592096409667D-03
2	42	0.2534095506899352D-03	0.3505035342285137D-03	0.7129742782372550D-03
3	78	0.2473114711669522D-03	0.3607138018058794D-03	0.7936052278053867D-03
4	138	0.2445714254542476D-03	0.3701802501488918D-03	0.8591464052345034D-03
5	222	0.2337583505325639D-03	0.3375931456911586D-03	0.7918101347523176D-03
6	330	0.2253173665961850D-03	0.3105604155630747D-03	0.7325557688296332D-03
7	462	0.2092777698103482D-03	0.2447446052984088D-03	0.5464419176391876D-03
8	618	0.1981310492965937D-03	0.1968803334211282D-03	0.4054869521310821D-03

Throughout this paper, to measure the error of the finite element solutions, we use the following definition:

$$\|\mathcal{E}\|_{E,r} = \left[\frac{|\mathcal{U}(\{u_{ex}\}) - \mathcal{U}(\{u_{FE}\})|}{\mathcal{U}(\{u_{ex}\})} \right]^{1/2}.$$ (48)

That is, it is the square root of the difference between the true strain energy and the computed strain energy divided by the true strain energy. It was shown in ([36]) that $\|\mathcal{E}\|_{E,r}$ is actually **the relative error in the energy norm**, provided that one of the following cases applies: all Boundary conditions are either homogeneous Dirichlet or arbitrary Neumann boundary conditions; some Dirichlet boundary conditions are nonhomogeneous, but all other boundary conditions are either homogeneous Neumann or homogeneous Dirichlet and the governing equations are homogeneous. Moreover all examples in this section are one of these cases. Hence in what follows we will call $\|\mathcal{E}\|_{E,r}$ the relative error in the energy norm.

For the various wedge angles α, the total strain energies on $\Omega_2^{(\alpha)}$ obtained by applying MAM on Mesh I, shown in Fig. 5.4, are given in Table 5.3. The relative errors in the energy norm(%) are given in Fig. 5.6. By comparing with the true solutions, we can conclude that MAM is able to yield accurate solutions at virtually no extra cost, no matter how strong singularity the problem contains.

In order to compare the results obtained by MAM with those obtained by the mesh refinement method, Mesh I of 4 elements(see, Fig. 5.4.) are refined by putting circular layers of radii $\sigma, \sigma^2, \sigma^3, \sigma^4, \sigma^5, \sigma^6, \sigma^7, \sigma^8$, centered at the origin, where $\sigma = 0.15$ (which is known to be an optimal geometric ratio for a geometric mesh refinement for the h-p version of FEM). The refined mesh obtained by putting 2, 3, 4, ..., 9 layers will be denoted by Mesh II, Mesh III, Mesh IV,..., and Mesh IX, respectively. These meshes have 6, 8, 10, 12,...,, 20 elements respectively. For example, Mesh V is as shown in Fig. 5.5.

The strain energy, obtained by applying the standard FEM with the refined Mesh V to the problems on the domain $\Omega_2^{(\alpha)}$ are given in Table 5.4. And their relative errors in the energy norm, $\|\mathcal{E}\|_{E,r}$, computed by using the true strain energy are shown in Fig. 5.7.

Remark 5.1. The energy reported in the tables 5.3, 5.4, 5.5 are not monotone with p. This is caused by the fact that the boundary condition is imposed only approximately. For higher p this error has small influence and the energy decreases as it would occur if the (essential) boundary condition would be exactly imposed.

Table 5.4 and Fig. 5.7 show that the mesh refinement method can handle the weaker singularities. However it fails to give any practical solution of elasticity problems with very strong singularities such as the cases when $\alpha > 75°$. In order to show this fact vividly, the standard FEM is applied to the case when $\alpha = 89°$ with further refined

meshes; Mesh I, Mesh III, Mesh V, Mesh VII, and Mesh IX. The computed strain energies for those geometrically refined meshes are given in Table 5.4 and Table 5.5 and their relative error in the energy norm are shown in Fig. 5.8. In this case, by the massive geometric mesh refinements, finite element solutions are improved a little bit. However, the accuracy is not acceptable at all. In other words, the h-p version of the FEM fails for this problem.

Remark 5.2. (1) Even Though $\beta = \alpha/(90 - \alpha)$ is an optimal mapping size for the problems on the domain $\Omega_2^{(\alpha)}$, MAM with other choice of mapping size yields approximate solutions of practical accuracy. Actually MAM with mapping size (> 100) yields the relative error in the energy norm $\leq 3\%$ when the order of basis functions is 8 and Mesh I is used for the problem on the domain $\Omega_2^{(89)}$.

(2) It is worth noting that MAM can handle the elasticity problems even when the boundaries of the neighborhoods of their singularities are imposed by non-homogeneous essential boundary conditions.
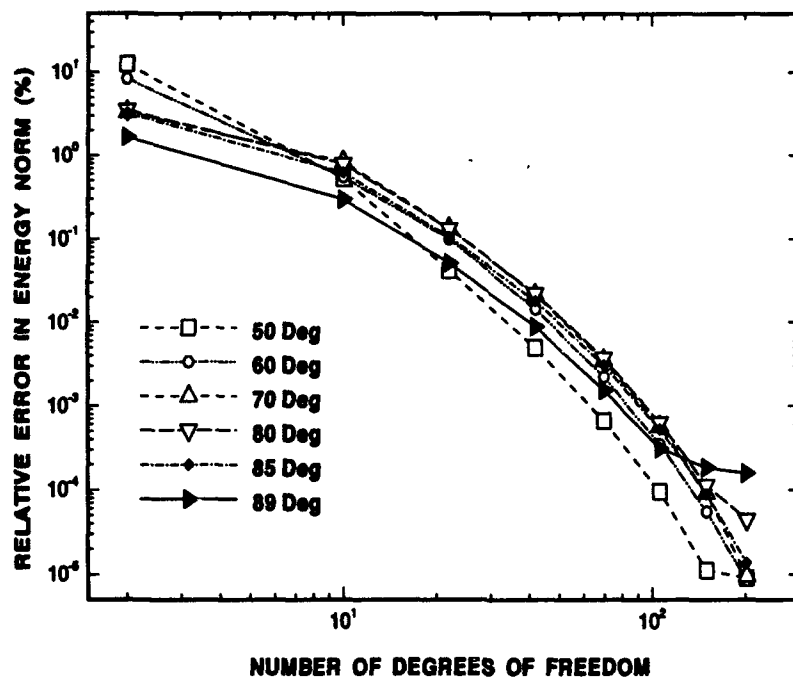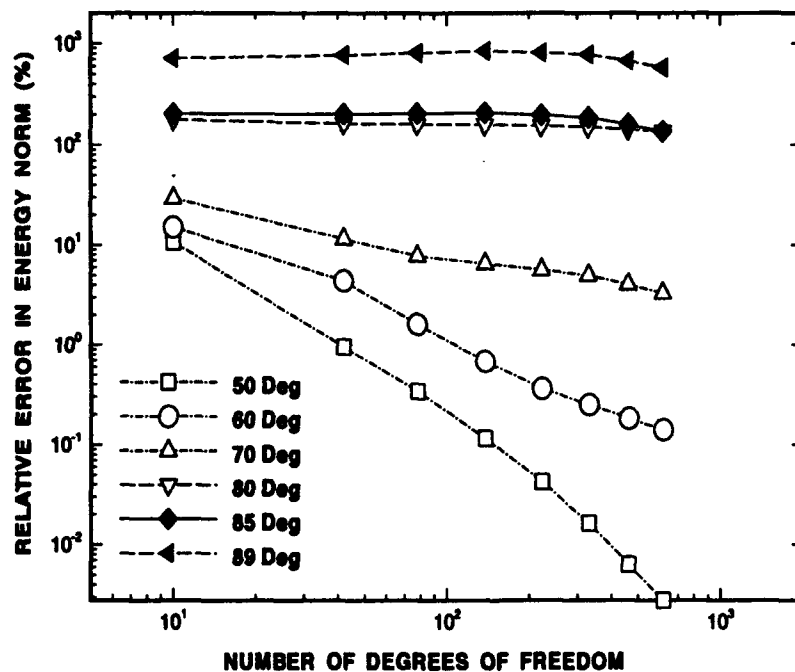

Fig. 5.6. The relative error in the energy norm(%) when MAM is applied with Mesh I.

Table 5.5. The strain energies on the domain $\Omega_2^{(89)}$ obtained without applying MAM.

p-deg	DOF	Mesh I	DOF	Mesh III
1	2	0.8348764761969085D-03	6	0.6720455342291412D-03
2	10	0.8363598689554478D-03	26	0.7753691417481764D-03
3	22	0.9184008854068470D-03	50	0.8631892906394158D-03
4	42	0.9931577497683493D-03	90	0.9345644101368223D-03
5	70	0.9137775851488808D-03	146	0.8612360703348015D-03
6	106	0.8430469500300520D-03	218	0.7967076857397165D-03
7	150	0.6223823176457848D-03	406	0.5940288770994173D-03
8	202	0.4550174531945867D-03	510	0.4405282879009032D-03

p-deg	DOF	Mesh VII	DOF	Mesh IX
1	14	0.5688829276912590D-03	16	0.5235413474168798D-03
2	58	0.6556907603472391D-03	72	0.6030890129562007D-03
3	106	0.7297117726166816D-03	132	0.6710403386777638D-03
4	186	0.7898923442515647D-03	232	0.7262984181673099D-03
5	298	0.7280587060296026D-03	372	0.6695176825383317D-03
6	442	0.6736470524085897D-03	552	0.6195529458233573D-03
7	618	0.5027442583422036D-03	772	0.4626180089851831D-03
8	826	0.3733095376025999D-03	1032	0.3437619833159763D-03

Fig. 5.7. The relative error in the energy norm(%) on the domains $\Omega_2^{(\alpha)}$ for $\alpha = 50, 60, 70, 80, 85, 89$ when the p-version of FEM is applied with Mesh V.

27
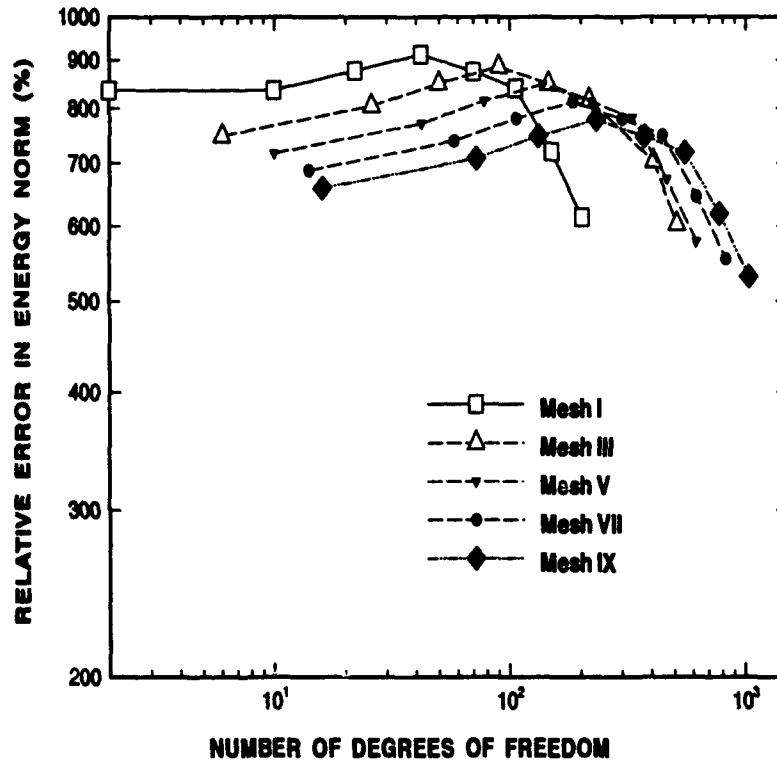
Fig. 5.8. The relative error in the energy norm(%) when the h-p version of the Finite Element Method is applied for the problem on the wedge domain $\Omega_2^{(\alpha)}$ of $\alpha = 89°$.

In the first two examples, the smallest eigenvalues λ were known. Thus, it was possible to choose an optimal mapping size $\beta = 1/\lambda$. However, in engineering practices, the exact eigenvalues, which represent the intensity of singularities, are not known in advance. The next two examples demonstrate that MAM succeeds in yielding good approximate solutions even for these cases.

Example 5.III. Let us consider the equations of elasticity on a domain Ω_3 shown in Fig. 5.9, which is isotropic with material constants; $E = 1000$ and $\nu = 0.3$. Suppose the boundary conditions are given as follows:

(1) $u_n = 0, u_t = 0$ (fixed) along $\Gamma_1 \cup \Gamma_2$,

(2) $T_n = 10, T_t = 2$ along Γ_5,

(3) $T_n = 0, T_t = 0$ (traction free) along $\partial\Omega\backslash(\Gamma_1 \cup \Gamma_2 \cup \Gamma_5)$.

Then it follows from the arguments in §3.1 that this problem has singularities at the crack tip $P_1(0,0)$ and the corner $P_2(2,2)$. Moreover, suppose the body force is zero, that is, $\{f\} = \{0,0\}^T$, then $\min\{Re(\lambda_j)\}$ are approximately 0.3 and 0.7 at $P_1(0,0)$ and $P_2(2,2)$ respectively.

28
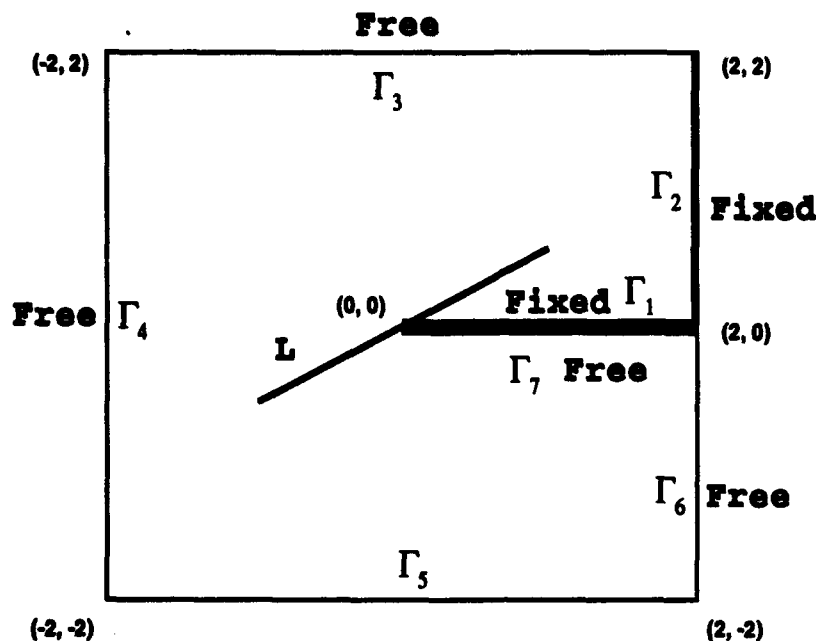
Fig. 5.9. The domain Ω_3 and the line segment L which is on the straight line $y = x(\tan \pi/8)$.

For the finite element approach, we construct two meshes, Mesh I and Mesh II on Ω as shown in Fig. 5.10. Mesh II is obtained from Mesh I by putting layers of radii $0.5, 0.5\sigma, 0.5\sigma^2, 0.5\sigma^3$ centered at P_1 and layers of radii $0.5, 0.5\sigma, 0.5\sigma^2$ centered at P_2, where $\sigma = 0.15$. Mesh I and Mesh II have 22 and 48 elements respectively. In Example 5.III, we use the mapping size $\beta = 6$ and $\beta = 2$ on the singular regions $S_1 = \{(x, y) : \|(x, y) - (0, 0)\| \leq 0.5\}$ and $S_2 = \{(x, y) : \|(x, y) - (2, 2)\| \leq 0.5\}$ respectively.

In Examples 5.III, " With Map " stands for the results obtained by applying MAM on Mesh I. " No Map " and " 48EL " stand for the results obtained by the standard Finite Element Method on Mesh I and Mesh II respectively without applying MAM.

The total strain energy obtained by the following three ways is listed in Table 5.6: the p-version of the FEM on Mesh I by applying MAM(With Map); the p-version of the FEM on Mesh I with no Map(No Map); the p-version of the FEM on Mesh II with no Map(48EL).
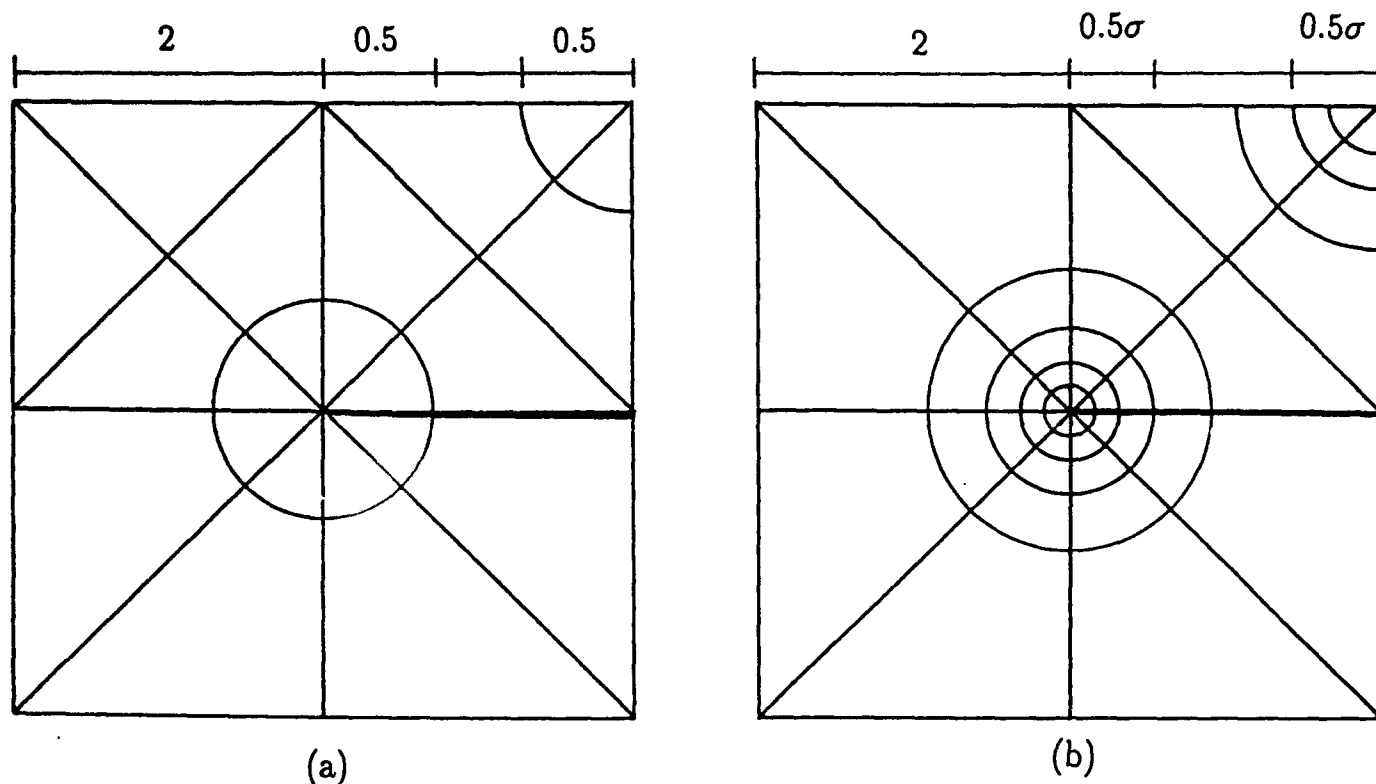
29

Fig. 5.10. (a) Mesh I (22 elements); (b) Mesh II (48elements).

Table 5.6. Total strain energy on Ω_3. when the body force is zero.

p-deg	With Map	48EL	No Map
1	1.702132029810480	1.656404349217337	1.231603737683330
2	2.061010428583605	2.018717728104414	1.605510783438384
3	2.093985634086386	2.063320794501468	1.736330296578600
4	2.110046396546211	2.082748318204508	1.815186503511321
5	2.113129774277219	2.089615423359967	1.864716288927604
6	2.113560741772014	2.093441297022001	1.899152183780876
7	2.113727076747088	2.096139989799332	1.925085281651720
8	2.113785840066801	2.098163679729239	1.945329260774251
9	2.113804271632455		

By applying the extrapolation approach given in Chapter 4 of ([36]) to the second column of Table 5.6 and the fourth column, DOF, of Table 5.7, we obtain $\mathcal{U}(u_{ex}) = 2.113815563245032$, the computed true total energy.

Table 5.7 is the relative error in strain energy(%) computed by applying the computed true energy to Table 5.6. And they are plotted in Fig. 5.11.

Table 5.7. Relative errors in the energy norm (%) and Degree of Freedom for the cases in Table 5.6.

p-deg	With Map	No Map	DOF	48EL	DOF
1	44.131	64.603	38	46.517	92
2	15.805	49.038	120	21.209	280
3	9.686	42.259	226	15.456	488
4	4.223	37.587	376	12.123	792
5	1.801	34.328	570	10.700	1192
6	1.098	31.867	808	9.818	1688
7	0.647	29.880	1090	9.144	2280
8	0.375	28.232	1416	8.605	2968
9	0.231		1786		

In this example, the displacements vary within very small ranges. Hence we can not see a clear distinction between "With Map" and "No Map" when their graphs are plotted. However, the differences are clear when the stresses are compared. As an example, the x-component (U) of the displacement and the equivalent stress (σ_e) at the points $(r, \pi/8)$, for $r = 0.9, 0.8, 0.7, 0.6, 0.4, 0.3, 0.2, 0.1$, and $-0.1, -0.2, -0.3, -0.4, -0.6, -0.7$ along the line $y = x \tan(\pi/8)$ are listed in Table 5.8.

The equivalent stresses along the line L(see, Fig. 5.9), given in Table 5.8, for three cases are plotted in Fig. 5.12. In case of applying MAM, the basis functions resemble the true solution around the singularities, hence the stresses near the singularity at $P_1(0,0)$ are very large. Actually, the equivalent stress at $P_1(0,0)$ is infinity. We plotted the graph of the equivalent stresses on $\Omega_* = [-2, -2] \times [-2, -0.1]$ in Fig. 5.13. In Fig. 5.13, the x-grid and y-grid sizes are 0.2 and 0.1 respectively. In this example, the equivalent stress of "With Map" is much bigger than "No Map" near the singularity at $P_1(0,0)$. One can notice this fact from Fig. 5.13.

The equivalent stresses along the line L(see, Fig. 5.9), given in Table 5.7, for three cases are plotted in Fig. 5.12. In MAM, the basis functions resemble the true solution around the singularities, hence the stresses near the singularity at $P_1(0,0)$ are very large. Actually, the equivalent stress at $P_1(0,0)$ is infinity. We plotted the graph of the equivalent stresses on $\Omega_* = [-2, -2] \times [-2, -0.1]$ in Fig. 5.13. In Fig. 5.13, the x-grid and y-grid sizes are 0.2 and 0.1 respectively. In this example, the equivalent stress of "With Map" is much bigger than "No Map" near the singularity at $P_1(0,0)$. One can see this fact from Fig. 5.13.
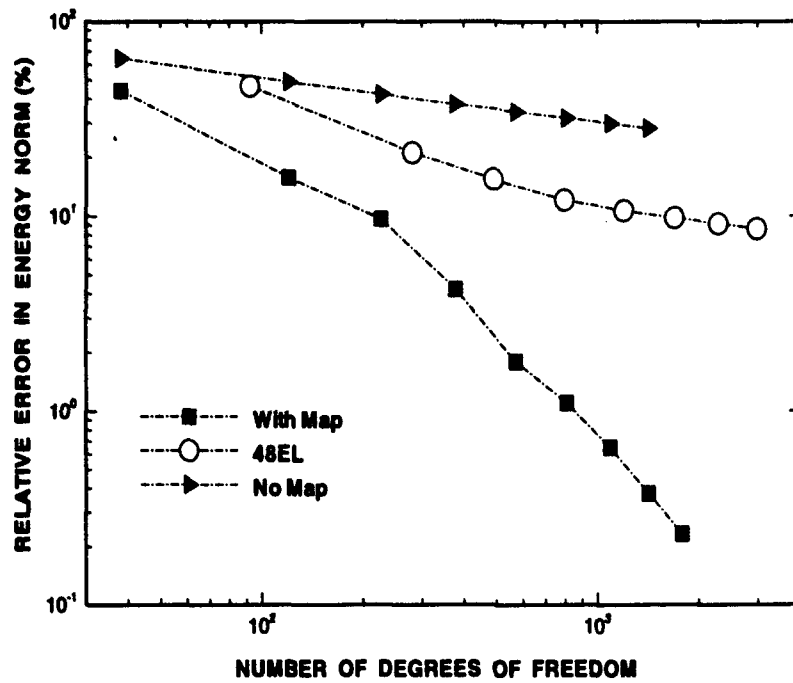
Fig. 5.11. Relative error in the energy norm(%) for the domain Ω_3 containing two corner singularities.
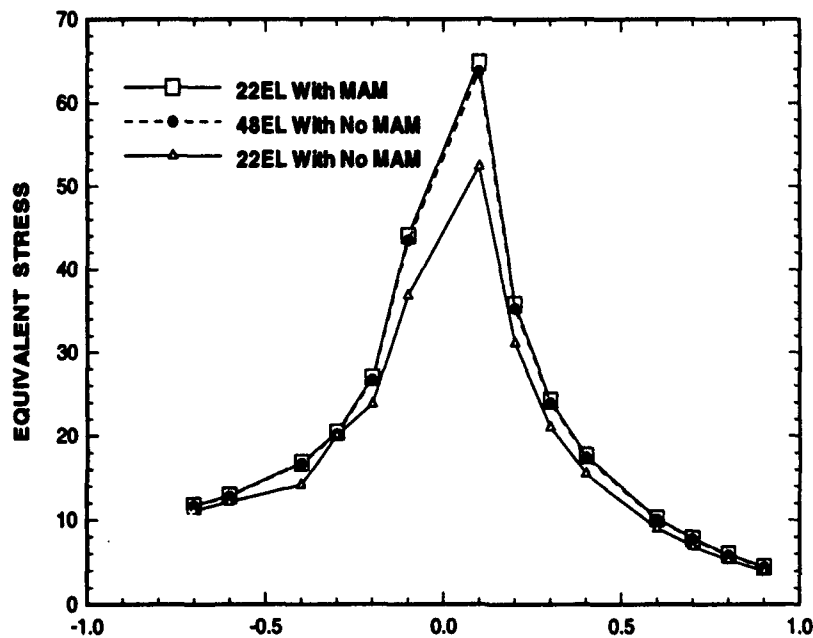

Fig. 5.12. The equivalent stress along the line L shown in Fig. 5.9. The scale on the horizontal axis represents the radius r of the polar coordinates $(r, \pi/8)$ of the points on L. For these computations, basis functions of order 8 are used.
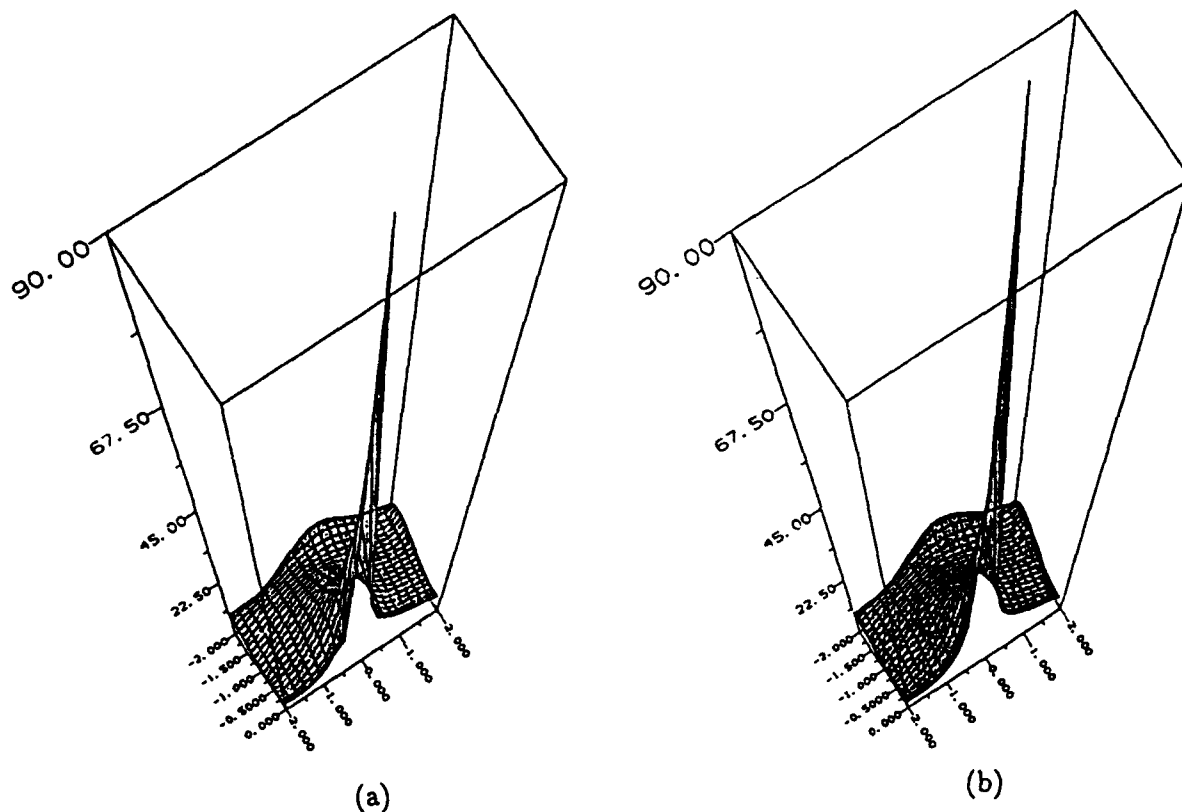
32

Fig. 5.13. The graph of equivalent stress on $\Omega_* = [-2, 2] \times [-2, -0.1]$: (a) No Map: (b) With Map. The x-grid and the y-grid sizes are 0.2 and 0.1 respectively. The order of basis functions used for this computation is 8.

Table 5.8. Equivalent stress (σ_e) the displacement (U: x-displacement) along the line L in Fig. 5.9. For these computations, basis functions of order 8 are used.

r	With Map		No Map		48EL	
	U	σ_e	U	σ_e	U	σ_e
0.9	6.836E-6	4.421	-2.153E-4	3.945	-1.361E-5	4.375
0.8	2.516E-4	5.897	-1.243E-6	5.234	2.280E-4	5.833
0.7	5.075E-4	7.762	2.226E-4	6.874	4.806E-4	7.678
0.6	7.695E-4	10.147	4.501E-4	8.972	7.391E-4	10.038
0.4	1.289E-3	17.647	8.953E-4	15.504	1.252E-3	17.452
0.3	1.535E-3	24.220	1.090E-3	21.029	1.493E-3	23.936
0.2	1.754E-3	35.811	1.250E-3	31.129	1.705E-3	35.338
0.1	1.908E-3	64.809	1.292E-3	52.415	1.848E-3	63.761
-0.1	2.003E-2	44.053	1.547E-2	36.843	1.963E-2	43.508
-0.2	2.253E-2	26.962	1.891E-2	23.818	2.218E-2	26.716
-0.3	2.430E-2	20.401	2.072E-2	20.083	2.397E-2	20.217
-0.4	2.576E-2	16.809	2.251E-2	14.149	2.546E-2	16.687
-0.6	2.831E-2	12.881	2.524E-2	12.135	2.803E-2	12.791
-0.7	2.949E-2	11.660	2.650E-2	11.066	2.921E-2	11.636

33

So far we have considered the corner singularities on isotropic elastic bodies. However, the interface singularity caused by an abrupt change in material properties in an elasticity problem has a similar structure to that of the corner singularity. However, the interface singularities are usually more complex and stronger than the corner singularities. In order to show that MAM can also handle this type of singularity, our next example concerns an elasticity problem with two interfaces.

Example 5.IV. Consider the equations of elasticity on the domain Ω_4 shown in Fig. 5.14 that is composed of three isotropic materials. That is, $\Omega_4 = \Omega_{41} \cup \Omega_{42} \cup \Omega_{43}$, and the material constants on each subdomain are given in the following table:

	On Ω_{41}	On Ω_{42}	On Ω_{43}
E	1000	10	1000
ν	0.1	0.001	0.3

We also assume that it has a nonzero body force, $\{f\} = \{10, 1000\}^T$.
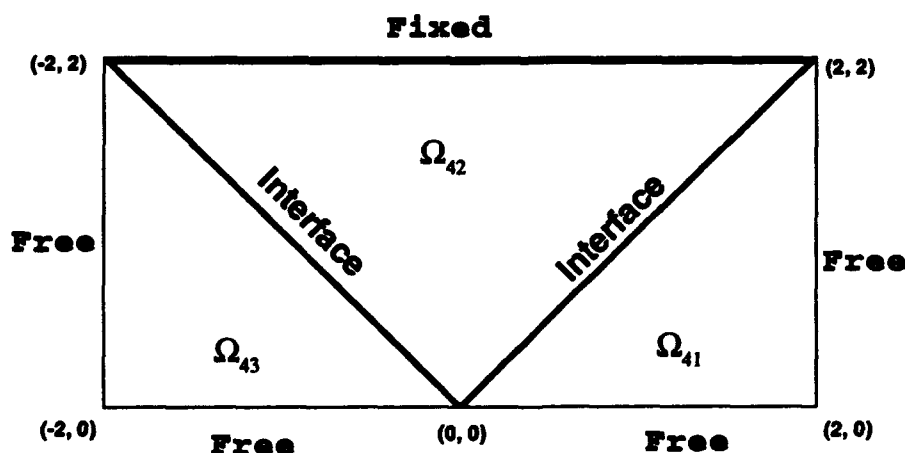
Fig. 5.14. The domain Ω_4 for the interface problem with two interfaces.

This interface problem has singularities at $P_1(0,0), P_2(2,2)$, and $P_3(-2,2)$. Thus we choose the neighborhoods S_j of the singularities as follows: $S_j = \{(x,y) : \|(x,y) - P_j\| \leq$

34

$0.5\}, j = 1, 2, 3$. A mesh on Ω_4 that is compatible with these neighborhoods of the singularities are shown in Fig. 5.15.

The success of the Method of Auxiliary Mapping depends on the choice of *the mapping size* β of the auxiliary mapping. In our method, a circular sector, $S = \{(r, \theta) : 0 \leq \theta \leq \theta_0, r \leq r_0\}$, is mapped onto $S^* = \{(r^*, \theta^*) : 0 \leq \theta^* \leq \theta_0/\beta, r^* \leq r_0^{1/\beta}\}$, by the mapping $\varphi^{-1}(r, \theta) = r^{1/\beta}(\cos\theta/\beta, \sin\theta/\beta)$. Thus, if the mapping size, β, is very large then the mapped region will consist of very narrow circular sector elements. Nevertheless the convergence theorem given in the previous section still holds since these elements satisfy the maximal angle condition ([3]) which allows one angle to be arbitrarily small.

In this example, "$\beta = (\beta_1, \beta_2, \beta_3)$" means the results obtained by applying MAM with the auxiliary mappings of size $\beta_1, \beta_2, \beta_3$ for the singular regions S_1, S_2, S_3 respectively. In particular, "$\beta = (1, 1, 1)$" stands for the case when no mapping technique is used. The total strain energy obtained by the various choices of mapping sizes are listed in Table 5.9.

Table 5.9. Total strain energy for the interface problem.

p-deg	$\beta = (8, 10, 10)$	$\beta = (5, 10, 10)$	DOF
1	123032.2828452089	123284.2678773375	38
2	150287.7980849437	152583.4051500356	116
3	158804.9631362990	159786.2535574225	210
4	161232.7426132401	161314.8716586071	344
5	161708.1813612756	161697.6525341540	518
6	161749.2509783793	161745.8457528930	732
7	161760.1348046330	161758.1355019662	986
8	161761.8532415435	161760.3221783005	1280
9	161762.9347649495	161761.8908487467	1614

p-deg	$\beta = (5, 5, 5)$	$\beta = (1, 1, 1)$	DOF
1	116027.58299108	58106.6173116895	38
2	150578.57685495	88079.9225407295	116
3	158821.08704690	97828.5205550101	210
4	160167.37006738	104140.5899691367	344
5	160742.79149754	108695.2364448717	518
6	161051.55851408	112211.9290644471	732
7	161239.18068546	115041.7425766592	986
8	161361.96325978	117386.4326246329	1280

35

Fig. 5.15. A mesh for using MAM on the domain Ω_4 with two interfaces.

As before, extrapolating the second column of Table 5.9 gives

$$\mathcal{E}(u_{ex}) = 161765.7679239559$$

as the computed true total energy.
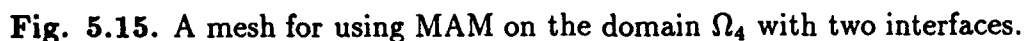
Table 5.10 is the relative error in the energy norm(%) computed by using this true energy and Table 5.9. And these relative errors in the energy norm versus the number of degrees of freedom are plotted in Fig. 5.16.

Table 5.10. The relative error in the energy norm (%) and Degree of Freedom for the cases in Table 5.8.

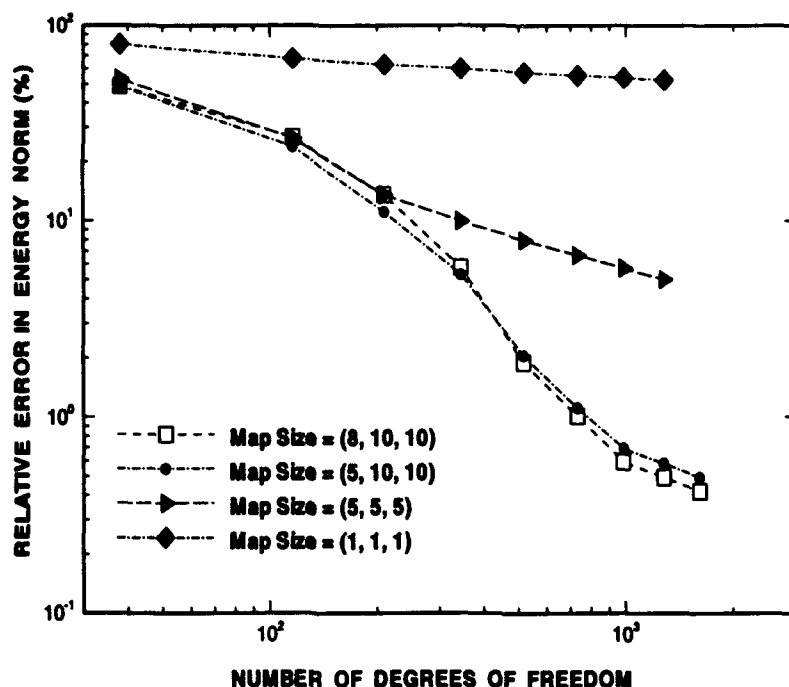| p-deg	$\beta = (8, 10, 10)$	$\beta = (5, 10, 10)$	$\beta = (5, 5, 5)$	$\beta = (1, 1, 1)$	DOF
1	48.933	48.773	53.173	80.050	38
2	26.637	23.825	26.300	67.491	116
3	13.529	11.062	13.492	62.869	210
4	5.740	5.280	9.940	59.685	344
5	1.887	2.052	7.952	57.277	518
6	1.010	1.110	6.645	55.347	732
7	0.590	0.690	5.705	53.743	986
8	0.492	0.580	4.996	52.377	1280
9	0.418	0.490			1614

36

Fig. 5.16. Relative error in the energy norm (%) for the interface problem.

Due to the large body force, we can see a big distinction between $\beta = (8, 10, 10)$ and $\beta = (1, 1, 1)$ even in the displacements. The graphs the y-displacement for the two cases, $\beta = (8, 10, 10)$ and $\beta = (1, 1, 1)$, are plotted in Fig. 5.17. Once again, the stresses obtained by using MAM is larger than the stresses obtained by the standard FEM at the neighborhoods of singularities. Numerical experiments show that the singularities at $P_2(2, 2)$ and $P_3(-2, 2)$ are much stronger than that at $P_1(0, 0)$.

From Table 5.9 and Table 5.10, we can conclude that the mapping size $\beta_2 = 5$ is not big enough for the singularity at P_2. On the other hand, experiments show that the mapping sizes $\beta_1 = 10$ and $\beta_2 = 15$ are too big for the singularities at P_1 and P_2 respectively.

Remark 5.3. In all cases except the second example we had natural boundary conditions and hence the energy increases with p.

(a)   (b)
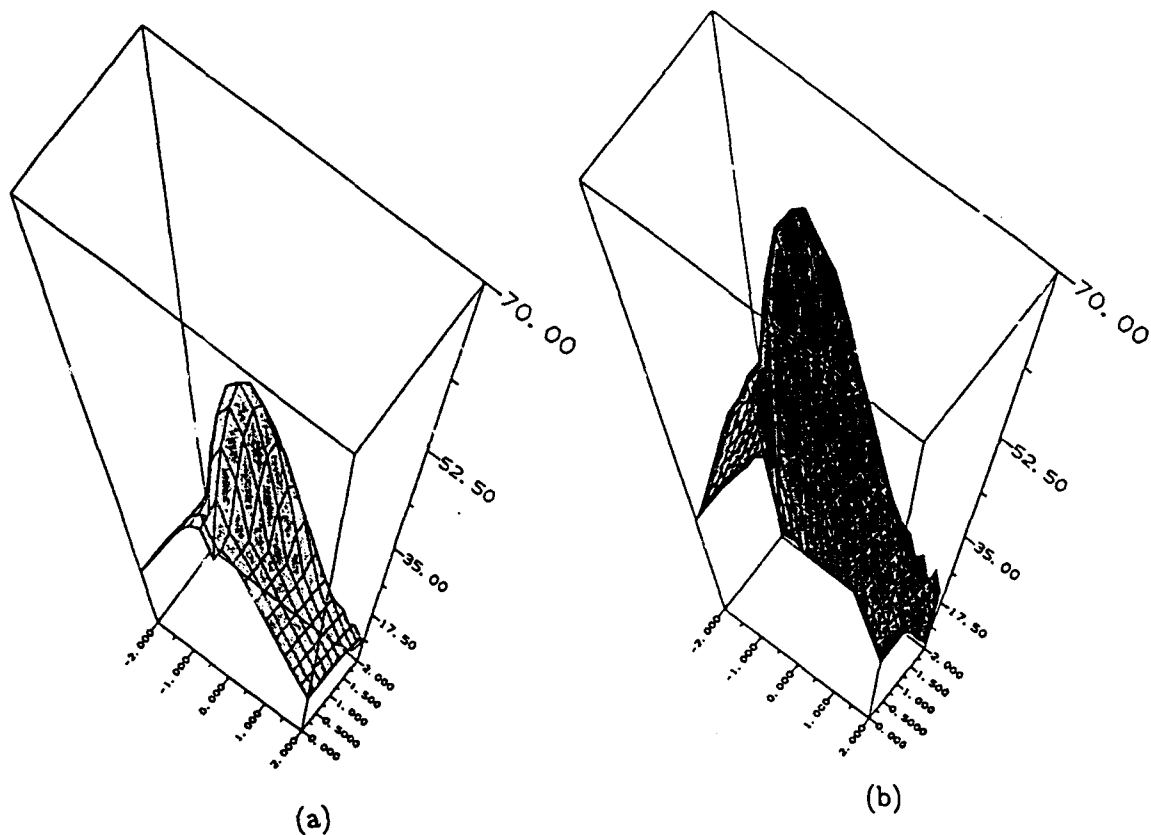
Fig. 5.17. The graph of the y-displacement over $\Omega = [-2,2] \times [0,2]$: (a) No Map; (b) With MAM. The x-grid and y-grid sizes are 0.2 and 0.1 respectively. The order of basis functions used for this computation is 8.

If an oversized auxiliary mapping (i.e. $\beta \gg (\min\{Re(\lambda)\})^{-1}$) were used in MAM, then one cannot see the expected improvement until the polynomial degree is of high order. It was shown in ([8]) that if larger mapping size is selected, then one must choose higher degree basis polynomials to get large improvement in accuracy. Hence, from a practical point of view an optimal choice for the mapping size at each singular region is $\beta = (\min\{Re(\lambda_j)\})^{-1}$. Thus, in order to obtain optimal results from MAM, it is desirable to know the eigenvalues λ at each singularity. Actually, it can be computed by solving trigonometric equations given in §2.1 for the corner singularity or by using the computer code given in ([31]) for the interface singularity. Even if we do not have prior knowledge of the eigenvalues, MAM, using an auxiliary mapping of any size $\beta > 1$, will always yield a large improvement. In fact, since an oversized auxiliary mapping yields better results than undersized auxiliary mapping (unless the basis functions are

38

of very low degree), it is better to start with a large β, for example $\beta = 10$ in such a case. Another possibility is to use different strengths of mappings and select the one which leads to the largest strain energy.

6 Concluding Remarks

MAM can efficiently handle the plane elasticity problems containing such singularities as corner and interface singularities. No matter how strong singularities the problem contains, MAM yields an accurate solution at vitually no extra cost if the structures of singularities are known. Actually MAM can handle the elasticity problems which even can not be solved by the h-p version of the Finite Element Method. In applying MAM, an optimal results can be obtained if the structure of the singularities are known. However, even if the prior knowledge on the singularities are not known, MAM can yield very reasonable solutions to any plane elasticity problems with singularity.

References

[1] Akin, J. E.: *The Generation of Elements with Singularities,* Int. J. Numer. Meth. Eng., **10**, pp. 1249-1259 (1976).

[2] Akin, J. E.: *Elements for the Analysis of Line Singularities,* The Mathematics of Finite Elements with Applications, **3**, ed. J.R. Whiteman, Academic Press, London, 1979.

[3] Babuška and Aziz, A.K. :*On the Angle Condition in the Finite Element Method,* SIAM J. Numer. Analysis, **13**, 214-226(1976).

[4] Babuška, I. and Guo, B.: *The h-p Version of the Finite Element Method For Domains with Curved Boundaries,* SIAM J. Numer. Anal., **25**, pp. 837-861 (1988).

[5] Babuška, I. and Guo, B.: *The h-p Version of the Finite Element Method For Problems with Nonhomogeneous Essential Boundary Condition,* Methods Appl. Mech. Engrg. **74** , pp 1-28 (1989).

[6] Babuška, I. and Guo, B.: *Regularity of the Solutions of Elliptic Problem with Piecewise Analytic data, part I: Boundary Value Problems for Linear Elliptic Equation of Second Order,* SIAM J. Math. Anal., **19**, pp. 172-203 (1988).

[7] Babuška, I., Kellogg, B. and Pitkäranta, J.: *Direct and Inverse Error Estimates for Finite Elements with Mesh Refinements,* Numer. Math. **33**, pp. 447-471 (1979).

[8] Babuška I. and Oh, H.-S.: *The p-Version of the Finite Element Method for Domains with Corners and for Infinite Domains,* Numer. Meth. PDEs, **6**,pp. 371-392 (1990).

[9] Babuška, I. and Rosenzweig, M. R.: *A Finite Element Scheme for Domains with Corners,* Numer. Math. **20**, pp. 1-21 (1972).

[10] Babuška, I. and Suri, M. :*The Optimal Convergence Rate of the p-Version of the Finite Element Method,* SIAM J. Numer. Anal. **24**, No. 4 , pp. 750-776 (1987).

[11] Babuška, I. and Suri, M.: *The h-p Version of the Finite Element Method with Quasi-uniform Meshes,* Math. Modelling and Numer. Anal. **21**, pp 199-238(1987).

[12] Babuška, I., Szabo, B. A. and Katz, I. N.: *The p-Version of the Finite Element Method,* SIAM J. Numer. Anal. **18**, pp. 515-545 (1981).

[13] Ciarlet, P. G.: *The Finite Element Method for Elliptic Problems,* North-Holland, Amsterdam, 1978.

[14] Gordon,W. and Hall,C.: *Construction of Curvilinear Co-ordinate Systems and Applications to Mesh Generation,* Int. J. Numer. Meth. Eng., **7**, 461-477 (1973).

[15] Grisvard, P.: *Elliptic Problems in Nonsmooth Domains*, Pitman Publishing Inc. 1985.

[16] Gui, W. and Babuška, I.: *The h, p, h-p Versions of the Finite Element Method in 1 Dimension, Part 1: The Error Analysis of the p-Version;* , Numer. Math., **49**, pp. 577-612 (1986).

[17] Gui, W. and Babuška, I.: *The h, p,h-p Versions of the Finite Element Method in 1 Dimension, Part 2: The Error Analysis of the h and h-p Versions,* Numer. Math., **49**, pp. 613-657 (1986).

[18] Gui, W. and Babuška, I.: *The h, p, h-p Versions of the Finite Element Method in 1 Dimension, Part 3: The Adaptive h-p Version,* Numer. Math., **49**, pp. 659-683 (1986).

[19] Guo, B. and Babuška, I.: *The h-p Version of the Finite Element Method. Part 1: The Basic Application Results,* **1**, pp. 21-41 (1986).

[20] Guo, B. and Babuška, I.: *The h-p Version of the Finite Element Method, Part 2: General Results and Applications,* Computat. Mech., **1**, pp. 203-220 (1986).

[21] Guo, B. and Oh, H. S.: *The h-p Version of the Finite Element Method for Problems with Interfaces,* to appear in Int. J. Numer. Meth. Eng. (1994)

[22] Fix, G., Gulati, S. and Wakoff, G. I.: *On the Use of Singular Functions with the Finite Element Method,* J. of Comp. Physics, **13**, pp. 209-228 (1973).

[23] Han, H. :*The Numerical Solutions of Interface Problems by Infinite Element Method,* Numer. Math. **39**, pp. 39-50 (1982).

[24] Hendry, J.A. and Delves L. M.: *Global Element Method Applied to a Harmonic Mixed Boundary Value Problem,* J. Comp. Phys., **33**, pp 33-44 (1979).

[25] Karp, S.N. and Karal, F.C. : *The Elastic-Field Behavior in the neighborhood of a Crack of Arbitrary Angle,* Comm. Pure and Applied Math., **15**, pp 413-421, (1962).

[26] Kellogg, R.B. : *On the Poisson Equation with Intersecting Interfaces,* Applicable Analysis, **4**, pp. 101-129(1975).

[27] Kondrat'ev, V. A.: *Boundary Problems for Elliptic Equations with Conical or Angular Points,* Trans. Moscow Math. Soc., **16**, pp. 227-313 (1967).

[28] Lucas, T.R. and Oh, H.-S. : *The Method of Auxiliary Mappings in the Finite Element Solutions of Elliptic Boundary Value Problems Containing Boundary or Corner Singularities,* J. of Comp. Physics **108**, pp327-432 (1993).

[29] Li, Z.C. and Mathon, R.: *Error and Stability Analysis of boundary Methods for elliptic Problems with Interfaces,* Math. Com. **54**, pp 41-61 (1990).

[30] Oh, H.-S. and Babuška, I. : *The p-version of the Finite Element Method for Elliptic Boundary Value Problems with Interfaces,* Comp. Meth. Appl. Mech. Engrg, Vol. 97, pp 211-231 (1992).

[31] Papadakis, P.:*Computational Aspects of the Stress Intensity Factors for two-dimensional Elasticity,* Doctoral Dissertation, University of Maryland,(1989).

[32] Parton, V.Z. and Perlin, P.I.: Mathematical Methods of the Theory of Elasticity, Volume 1, MIR publishers Moscow, 1984.

[33] Rank, E. and Babuška, I.: *An Expert System for Optimal Mesh Design in the h-p Version of the Finite Element Method,* Int. J. Numer. Meth. Eng., **24**, pp 2087-2106 (1987).

[34] Stern, M.:*Families of Consistent Conforming Elements with Singular Derivative fields,* Int. J. Numer. Meth. Eng., **14** , pp. 409-421 (1979).

[35] Strang, G. and Fix, G.: *An Analysis of the Finite Element Method,* Prentice-Hall, 1973.

[36] Szabó, B. and Babuška, I. : Finite Element Analysis, John & Wiley , 1990.

[37] Thatcher, R.W.: *The Use of Infinite Grid Refinements at Singularities in the Solution of Laplace's Equation,* Numer. Math., **25**, pp. 163-178 (1976).

[38] Tsamasphyros, G.: *Singular Element Construction Using a Mapping Technique,* Int. J. Numer Meth. Eng., **24**, pp. 1305-1316 (1987).

The Laboratory for Numerical Analysis is an integral part of the Institute for Physical Science and Technology of the University of Maryland, under the general administration of the Director, Institute for Physical Science and Technology. It has the following goals:

To conduct research in the mathematical theory and computational implementation of numerical analysis and related topics, with emphasis on the numerical treatment of ar and nonlinear differential equations and problems in linear and nonlinear algebra.

To help bridge gaps between computational directions in engineering, physics, etc., and those in the mathematical community.

To provide a limited consulting service in all areas of numerical mathematics to the University as a whole, and also to government agencies and industries in the State of Maryland and the Washington Metropolitan area.

To assist with the education of numerical analysts, especially at the postdoctoral level, in conjunction with the Interdisciplinary Applied Mathematics Program and the programs of the Mathematics and Computer Science Departments. This includes active collaboration with government agencies such as the National Institute of Standards and Technology.

To be an international center of study and research for foreign students in numerical mathematics who are supported by foreign governments or exchange agencies (Fulbright, etc.).

Further information may be obtained from Professor I. Babuška, Chairman, Laboratory for Numerical Analysis, Institute for Physical Science and Technology, University of Maryland, College Park, Maryland 20742-2431.